



ASSESSMENT MODEL FOR ESTUARINE CIRCULATION
AND SALINITY

Kurt W. Hess

Washington, DC
June 1985

NOAA TECHNICAL MEMORANDUMS

National Environmental Satellite Data and Information Services, Assessment and Information Services Center Subseries

The Assessment and Information Services Center provides value - added environmental information to support national needs and goals. The products and services of AISC's staff of environmental scientists, economists, librarians and information specialists, and computer specialists provide decision assistance to the nation's resource managers. AISC's programs in environmental assessments and environmental information management complement the data collection and archival program of other National Environmental Satellite Data and Information Services (NESDIS) components.

The Technical Memorandum series provides an informal medium for the documentation and quick dissemination of results not appropriate, or not yet ready, for formal publication in the standard journals. The series is used to report on work in progress, to describe technical procedures and practices, or to report to a limited audience.

These papers are available from the originating office and also from the National Technical Information Service (NTIS), U.S. Department of Commerce, 5285 Port Royal Road, Springfield, VA 22151. Prices vary for paper copy and microfiche.

NESDIS Technical Memorandum

- AISC 1 Assessment Models for Surface Dispersion of Marine Pollutants. Kurt W. Hess, Fred G. Everdale, and Peter L. Grose, May 1985.
- AISC 2 Comparison of Boundary Layer Winds from NWS LFM Output and Instrumented Buoys. Robert W. Reeves and Peter J. Pytlowany, May 1985.

NOAA Technical Memorandum NESDIS AISC 3

ASSESSMENT MODEL FOR ESTUARINE CIRCULATION
AND SALINITY

Kurt W. Hess

Washington, DC
June 1985

UNITED STATES
DEPARTMENT OF COMMERCE
Malcolm Baldrige, Secretary

National Oceanic and
Atmospheric Administration
Anthony J. Calio,
Deputy Administrator

National Environmental Satellite,
Data, and Information Service
John H. McElroy,
Assistant Administrator



CONTENTS

	Page
ABSTRACT	1
1. INTRODUCTION	1
2. THE MODEL FORMULATION	2
3. MODEL TESTING	6
4. PROTOTYPE CHESAPEAKE BAY MODEL	10
5. CONCLUSIONS AND FUTURE WORK	13
6. REFERENCES	14
APPENDIX I List of Symbols	16
APPENDIX II The Model Equations	17
TABLE	21
FIGURES	22

ASSESSMENT MODEL FOR ESTUARINE CIRCULATION AND SALINITY

Kurt W. Hess

Marine Environmental Assessment Division
Assessment and Information Services Center
National Environmental Satellite, Data, and
Information Service, Washington, DC 20235

ABSTRACT. A numerical model for three-dimensional time-dependent circulation and concentration is described. The mass and momentum equations are split into internal and external modes to save computer run time. A dimensionless vertical variable allows for a uniform number of levels at all cells in the square-grid mesh. The model was tested on cases representing tidal, wind, and density flow, and concentration distributions. Results from a prototype model of Chesapeake Bay tides and currents are included. Changes in salinity due to hurricane Agnes are discussed.

1. INTRODUCTION

The Marine Environmental Assessment Division has developed a three-dimensional numerical model for estuarine and coastal circulation. The model computes tidal, wind-driven, and density-driven currents in bays and coastal areas. The model is documented herein for informed user interaction, and the technique can be applied to problems involving the assessment of impacts of extreme weather and oceanic events on the marine environment.

Assessment of extreme environmental conditions frequently benefits from a knowledge of local water circulation patterns. Examples of this type of problem are marine pollution behavior, effects of bay-shelf exchanges on fishery recruitment, the dynamics of anoxic events, and extreme reductions or increases in estuarine salinity or temperature. The spatial variability of the relevant quantities which describe the system is best expressed in three dimensions. Each of these problems can benefit from the application of a numerical hydrodynamic model. In addition, the application of a circulation model to a particular area often leads to a deeper understanding of the physical processes which are important for the local dynamics. This knowledge helps both the qualitative overview of a complex system, and establishes quantitative limits on many of the variables which determine the state of the system.

Three-dimensional numerical models have been used routinely for the last several years. One of the best known of these is the Rand Corporation model developed by Leendertse and his colleagues (Liu and Leendertse, 1975), and applied to several coastal areas. Another well-known model was developed by Blumberg, Mellor, and associates (Blumberg and Mellor, 1981) at Dynalysis of Princeton, Inc. The Sheng (1983) model, developed for the U. S. Army Engineer Waterways Experiment Station, has been applied to the shallow shelf region of

the Louisiana-Mississippi coast. The major problems with the use of these models are the lack of documentation and the proprietary status of the computer code.

The computer model described here, MECCA (Model for Estuarine and Coastal Circulation Assessment), shares many of the features of other three-dimensional models. MECCA is designed to compute currents due to winds, tides, atmospheric pressure gradients, and density gradients at points on a grid mesh. The model solves the external, or barotropic, mode of water flow separately from the internal, or baroclinic, mode. The external mode circulation is computed using a vertically-integrated model to get the water level and flowrates (e.g. Hess and White, 1974). A dimensionless vertical coordinate is used so a uniform number of vertical levels occurs everywhere in the grid. The internal mode velocities and the concentrations are computed at all levels (e.g. Hess, 1975). Turbulent exchange is modeled as a local process without the transport of turbulent kinetic energy. The program was written to run in Fortran on a VAX 11/750 computer.

This report contains a brief description of the model, its equations, and some of its behavior. Further information can be found in Hess (1985a, b, c).

2. THE MODEL FORMULATION

The MECCA program is designed to simulate water currents with numerical finite-difference methods for coastal areas such as bays, estuaries, and the shallow waters of the continental shelf. The hydrodynamic equations for generalized fluid flow were the starting point for the development, but experience has shown that many of the terms in the equations represent processes which can be neglected for the specific type of flow we are studying. We have confined the application of the model to velocity and concentration distributions which are slowly varying in time and space. Changes in the horizontal direction are on the scale of hundreds of meters to kilometers, and in the vertical are on the scale of tens of centimeters. The time scale is on the order of hundreds of seconds. The small spatial scale allows the use of rectangular, rather than spherical, coordinates. Depths are limited to be of the same order of magnitude as the typical Ekman depth (tens of meters).

The computer program solves the equations of single-solute, variable-density water flow in shallow water in a right-handed coordinate system with the x-direction arbitrary, and the z-axis directed upward. The equations are the momentum balances for horizontal flow, the hydrostatic approximation, mass continuity, conservation of a solute, and an equation of state. Metric units, with a few exceptions, are used throughout the development. Salinity units are parts per thousand (ppt).

2.1 The Model Equations

The set of governing equations for water flow are used in MECCA. In the equations, a subscript comma followed by a parameter denotes partial differentiation with respect to that parameter. Multiple parameters in the subscript denote multiple differentiation. For example,

$$\partial u / \partial t = u_{,t} \quad \text{and} \quad \partial^2 u / \partial x^2 = u_{,xx}.$$

The dependent variables are the velocity components (u, v, w), the pressure (p), density (ρ), and concentration (c). For the most part the concentration represents salinity, although the development is general enough to represent temperature. Symbols are defined in Appendix I. The governing equations used in the model are as follows.

Horizontal velocity in the x-direction is given by

$$u_{,t} + (uu)_{,x} + (uv)_{,y} + (uw)_{,z} = -1/\rho_0 p_{,x} + fv + A_h(u_{,xx} + u_{,yy}) + (A_v u_{,z})_{,z} \quad (1)$$

Horizontal velocity in the y-direction is given by

$$v_{,t} + (vu)_{,x} + (vv)_{,y} + (vw)_{,z} = -1/\rho_0 p_{,y} - fu + A_h(v_{,xx} + v_{,yy}) + (A_v v_{,z})_{,z} \quad (2)$$

The hydrostatic equation is

$$p_{,z} = -\rho g. \quad (3)$$

The equation for water mass conservation is

$$u_{,x} + v_{,y} + w_{,z} = 0. \quad (4)$$

The equation of conservation of the solute is

$$c_{,t} + (uc)_{,x} + (vc)_{,y} + (wc)_{,z} - D_h(c_{,xx} + c_{,yy}) - (D_v c_{,z})_{,z} = 0 \quad (5)$$

The equation of state for water is

$$\rho = \rho_0(1 + \alpha c) \quad (6)$$

2.2 Boundary Conditions

Boundary conditions at the top and bottom horizontal surfaces are discussed first. The conditions for the horizontal velocities are the equality of stresses applied to the upper and lower surfaces. At the upper surface ($z = h$), the applied stress is due to the wind, and at the lower surface ($z = -d$) the applied stress is due to bottom friction. That is,

$$u_{,z} = T_{sx}, \quad v_{,z} = T_{sy} \quad \text{at } z = h, \quad (7)$$

$$u_{,z} = T_{bx}, \quad v_{,z} = T_{by} \quad \text{at } z = -d. \quad (8)$$

For the vertical velocity, the kinematic matching condition applies,

$$w = h_{,t} + uh_{,x} + vh_{,y} \quad \text{at } z = h, \quad (9)$$

$$w = uh_{,x} + vh_{,y} \quad \text{at } z = -d. \quad (10)$$

For the concentrations, the condition at each horizontal surface is

$$c_{,z} = I_c(x,y,z,t) \quad \text{at } z = h, \quad (11)$$

$$c_{,z} = 0 \quad \text{at } z = -d \quad (12)$$

The top boundary condition allows for an input at the atmospheric interface, which is non-zero if c is temperature. For salinity, $I_c = 0$.

At lateral boundaries, there are several possible conditions. If the boundary is a land-water interface, the velocity normal to the side is zero,

$$u = 0 \quad \text{at boundaries normal to the x-direction,} \quad (13)$$

$$v = 0 \quad \text{at boundaries normal to the y-direction.} \quad (14)$$

For the concentrations, the advective mass flux will automatically be zero, and the diffusive flux must vanish

$$D_h c_{,x} = 0 \quad \text{at boundaries normal to the x-direction,} \quad (15)$$

$$D_h c_{,y} = 0 \quad \text{at boundaries normal to the y-direction.} \quad (16)$$

If the lateral boundary is open, another set of conditions applies. At the ocean we can specify the water level

$$h = F_h(x,y,t) \quad (17)$$

or the velocities normal to the side,

$$u = F_u(x,y,z,t) \quad \text{at boundaries normal to the x-direction,} \quad (18)$$

$$v = F_v(x,y,z,t) \quad \text{at boundaries normal to the y-direction.} \quad (19)$$

The radiation boundary condition (Wurtele, et al., 1971) can be used to allow free waves to propagate out of the region:

$$h = U(gH)^{-1/2} \quad \text{at boundaries normal to the x-direction,} \quad (20)$$

$$h = V(gH)^{-1/2} \quad \text{at boundaries normal to the y-direction.} \quad (21)$$

The concentrations are also specified

$$c = F_c(x,y,z,t) \quad (22)$$

when the flow is coming into the domain of computation. If the flow is out, the condition is specified as a function of the local distribution

$$c_{,xx} = 0 \quad \text{at boundaries normal to the x-direction,} \quad (23)$$

$$c_{,yy} = 0 \quad \text{at boundaries normal to the y-direction.} \quad (24)$$

2.3 Stress Parameterization

The interfacial stresses are expressed in the following ways. The wind stress per unit water density (specific stress) at the upper surface is defined as

$$T_{sx} = rC_{aw}V_{10}V_x, \quad T_{sy} = rC_{aw}V_{10}V_y, \quad (25)$$

where r is the ratio of air and water density (here $r=0.00125$), and the drag coefficient (Wu, 1975) is

$$C_{aw} = 0.0008 + 0.000065 V_{10}. \quad (26)$$

Bottom specific stresses can have two forms. Allowing for a slip along the bottom, the specific stress is

$$T_{bx} = C_{wb} (u^2 + v^2)^{1/2}u, \quad T_{by} = C_{wb} (u^2 + v^2)^{1/2}v. \quad (27)$$

The nominal value for C_{wb} is 0.003. If the bottom condition is a zero velocity, the specific stress is taken as

$$T_{bx} = A_v u_{,z}, \quad T_{by} = A_v v_{,z} \quad (28)$$

2.4 Turbulent Parameterization

The turbulent exchange parameters need to be specified to complete the set of equations. The horizontal momentum exchange coefficient, A_h , is taken as a constant. The vertical momentum exchange coefficient, A_v , is taken as the product of a mixing length, the local velocity shear intensity, and a function of the Richardson number, Ri .

$$Ri = -g \rho_{,z} / \rho_0 (u_{,z} + v_{,z})^2 \quad (29)$$

$$A_v = [kz(h-z)] [(u_{,z} + v_{,z})^{1/2}] [(1 + C_1 Ri)^{-C_2}] \quad (30)$$

where k is von Karman's constant (0.40).

The horizontal mass exchange coefficient, D_h , is taken as a constant. The vertical exchange coefficient, D_v , is taken as a constant fraction, R_v , of the vertical momentum coefficient,

$$D_v = R_v A_v \quad (31)$$

Nominal values for C_1 , C_2 , and R_v are 5.0, 1.0, and 0.001, respectively.

2.5 Beta-Plane Formulation

The Coriolis parameter, f , is expressed by the beta-plane approximation,

$$f = f_0 + (x - x_0)[f_{,x}]_0 + (y - y_0)[f_{,y}]_0, \quad (32)$$

where (x_0, y_0) is a reference point in the grid mesh and f_0 is the Coriolis parameter at that point. Gradients of f are evaluated at the reference point. Both the x - and y -variations are needed because the grid axes are not necessarily aligned north-south.

2.6 Numerical Solution Techniques

The equations used in the computer program are developed from the set of governing equations (1 - 6) by a four-step process. First, the equations are integrated over the vertical to yield transport relations for the horizontal flowrates. Next, the transport relations are put into the form for mean velocity by dividing by the total depth. Then, the full three-dimensional momentum equations are subtracted from the mean velocity equations to give the internal-mode equations. Finally, the internal-mode equations are recast with the dimensionless vertical variable. The equations at each step of the process are listed in Appendix II.

The equations for the external mode are solved by an alternating-direction implicit finite-difference method, attributed to Abbott (Sobey, 1970) to augment numerical stability (Hess, 1985a). The non-linear advective terms are included as either forward or backward differences, depending on the direction of the current (Ramming and Kowalik, 1980). The internal mode velocities are then solved at each horizontal grid (Hess, 1985b). An implicit method calculates the horizontal internal-mode velocities (Hess, 1976), but not at each timestep so that computer run time is saved. The concentration is updated (Hess, 1985c) at each grid by solving (5) implicitly over z .

The equations are solved at points on a grid mesh of square elements with a gridsize denoted by ΔL and a timestep by ΔT . The variables are staggered in space (Fig. 1) to eliminate the build-up of short wavelength noise. Corner grids of triangular shape are permitted to better represent the coastline (Hess, 1985a). The model has 9 layers, and velocity and concentration variables at 10 levels.

3. MODEL TESTING

A number of test runs were made to refine the computational scheme and assess the behavior of the numerically-computed solution. In most cases the application of the model to a particular problem leads to a deeper understanding of the physics of the process. Changes in the numerical code were made with the physics and behavior of coastal currents in mind.

3.1 Tidal Flow

The first test was the comparison of the model output with the analytical solution for the case of forced oscillation of a semi-enclosed channel. The phenomenon is analogous to tidal forcing of a bay. The analytic solution given by Ippen and Harleman (1966) for water level and currents in a rectangular bay of length L and depth d without wind, bottom stress, non-linear advection, or

density variations, and driven by a tide of amplitude b (range = $2b$) and period T is as

$$h = (b/\cos(kL))\cos(2\pi t/T)\cos(kx) \quad (33)$$

$$u = -(2bC_0/d \cos(kL))\sin(2\pi t/T)\sin(kx). \quad (34)$$

The closed end of the basin is at $x=0$, and here $k=2\pi/L$ and $C_0=(gd)^{1/2}$. Figure 2 shows the comparison, which is excellent, for $g=9.81 \text{ m}^2/\text{s}$, $L=36 \text{ km}$, $\Delta L=6 \text{ km}$, $\Delta T=60 \text{ s}$, $T=6 \text{ h}$, and $d=10 \text{ m}$. Typical maximum differences between the two solutions are on the order of 0.001 m .

The results for the velocity comparison and for the case of a free oscillation in an enclosed basin were equally good.

3.2 Wind-driven Flow

Wind-driven currents are of great practical importance in bays and coastal areas. The next test case was the comparison of numerical and analytic solution for the steady-state current due to a constant wind blowing over shallow homogeneous water. For the case of zero velocity at the bottom, the analytic solution (Ekman, 1905) is

$$u = A\sinh(az)\cos(az) - B\cosh(az)\sin(az) \quad (35)$$

$$v = A\cosh(az)\sin(az) + B\sinh(az)\cos(az), \quad (36)$$

where

$$A = (T_{sy}/aA_v)[\cosh(ad)\cos(ad) + \sinh(ad)\sin(ad)]/[\cosh(2ad) + \cos(2ad)], \quad (37)$$

$$B = (T_{sy}/aA_v)[\cosh(ad)\cos(ad) - \sinh(ad)\sin(ad)]/[\cosh(2ad) + \cos(2ad)], \quad (38)$$

$$a = (f/2A_v)^{1/2}. \quad (39)$$

The origin is at the bottom of the water column. Figure 3a shows that the agreement is very good for the case of $T_{sx}=0$, $T_{sy}=0.000181 \text{ m}^2/\text{s}^2$, $d=11 \text{ m}$, $A_v=0.010 \text{ m}^2/\text{s}$, $L=6 \text{ km}$, $\Delta L=1000 \text{ m}$, $\Delta T=60 \text{ s}$, and $f=0.0001 \text{ s}^{-1}$. Differences are on the order of 0.003 m/s .

3.3 Density-driven Flow

Another test case involved the currents driven by a horizontal density gradient. This type of flow is important in partially-mixed estuaries. An analytic solution for the steady horizontal velocity with zero bottom current in complex form (Bishop and Overland, 1977) is

$$u + iv = (iag/f)(R_x + iR_y)[[\sinh((d+z)/a) - \cosh(z/a)]/\cosh(d/a) - z/d], \quad (40)$$

where $a = (A_v/if)^{1/2}$, and (41)

$$R_x = \rho_{,x}/\rho_0, \quad R_y = \rho_{,y}/\rho_0, \quad (42)$$

and there are no wind stresses or surface pressure gradients. The model results are very good, as shown in Fig. 3b, for $d=10$ m, $f=0.0001$ s⁻¹, $g=9.81$ m/s², $\Delta L=1000$ m, $\Delta T=60$ s; $A_v=0.01$ m²/s, $R_x=2.67 \times 10^{-7}$ (which corresponds to a horizontal salinity gradient of 0.33 ppt per km), and $R_y=0$. Differences are on the order of 0.005 m/s.

3.4 Non-Linear Velocity Advection

The non-linear advection terms in the flowrate equations (A.8, A.9) were tested by comparison with an analytic solution. The case we used, believed to be new, involved solving the simplified x-direction flowrate equation

$$(U^2)_{,x} + (C_{wb}/H) |U|U = 0 \quad (43)$$

The analytic solution we found, for the condition $U>0$, was

$$U = U_0 \exp[-(C_{wb}/2H)x] \quad (44)$$

A plot of the analytic and the model solutions is shown in Fig. 4. For this application we used $U_0=100$ cm/s, $C_{wb}=0.004$, $H=20$ m, $\Delta L=1000$ m, $\Delta T=60$ s, and $L=25$ km. The small differences are probably due to the non-centered approximation of the gradient term.

3.5 Horizontal Concentration Diffusion

A test of the diffusion calculations was performed with the simplified mass conservation equation

$$c_{,t} - D_h c_{,xx} = 0. \quad (45)$$

with a constant concentration, C_0 , at $x=0$. The analytic solution (Crank, 1956) is

$$c = C_0 \operatorname{erfc}[x/(4D_h t)^{1/2}] \quad (46)$$

The MECCA solution, after a simulated time of 32 h with $C_0=20$ ppt, is shown in Fig. 5, with $\Delta T=300$ s, $\Delta L=5000$ m, and $D_h=1000$ m²/s. The model solution closely matches the analytic solution, even in the leading region of low concentration.

3.6 Concentration Advection and Diffusion

The accuracy of the numerical solution of the concentration equation was tested on the case, believed to be new, of horizontal advection (from a vertically-varying velocity) balanced by vertical diffusion. That is

$$-u_0 \sin(\pi z/d) c_{,x} - D_v c_{,zz} = 0. \quad (47)$$

where the origin of the z-axis is at mid-depth. This type of flow, which is rightward along the bottom and leftward along the top, is similar to estuarine circulation. The author has found a solution for a constant-depth basin to be

$$c = C_1 - C_2 \sin(\pi z/d) - (D_v C_2 \pi^2 / u_0 d^2) x. \quad (48)$$

The comparison of the analytic and computed solutions for $C_1=20$ ppt, $C_2=-5$ ppt, $u_0=0.3$ m/s, and $D_v=0.0243$ m²/s in a rectangular basin, open at each end, with $d=20$ m, $\Delta L=5$ km, $\Delta T=300$ s, and $L=125$ km appears in Fig. 6. For this particular basin length, the concentration never becomes negative. At each end, the concentration was specified at all levels where the water was flowing into the basin. At the other levels, the concentration was extrapolated from the interior by assuming that c_x was constant across the boundary. The computed solution was quite smooth, and didn't show any evidence of the two-grid-length waves which often plague numerical schemes when advection is important. The computed solution in Fig. 6 was obtained after 480 h of simulation, from initial conditions substantially different from the steady-state solution. The error is on the order of 0.5 ppt. If we can define an advective time scale as

$$t' = L/u_0, \quad (49)$$

then the time required to approach the steady concentration distribution was on the order of $4t'$.

Two numerical approximations to the top and bottom conditions were tried. These were the first-order and the second-order one-sided differences at each boundary. The second-order scheme gave better results for this case, and so was used for the operational version of MECCA.

3.7 Conservation of Mass and Energy

The model was run for a large number of timesteps ($\Delta T = 30$ s) to determine the mass and energy conservation behavior. Several experiments were performed for circulation in a simulated enclosed basin of rectangular shape and constant depth. For a free-oscillation experiment, both total mass and solute mass balanced to within 1.0 % over several hundred timesteps. The energy calculations were more complicated, but the results were nearly as good. The simulation reproduced the well-known exchange of energy between the kinetic and potential forms. With the addition of bottom friction, the rate work per unit mass, W , done by the bottom stresses,

$$W_{,t} = uT_{bx} + vT_{by}, \quad (50)$$

integrated over the bottom area balanced the rate of change of the sum of kinetic and potential energy integrated over the volume.

Results were also good for the case of wind-driven circulation in an enclosed basin. Wind energy was added to the basin at the surface, and most of the energy was dissipated internally. A relatively small amount of energy was dissipated at the bottom, but the bottom stress transferred energy from the internal to the external mode. The external-mode energy was manifest in a simple oscillation.

Energy was conserved when the vertical mass exchange coefficient, A_v , was either a constant, or varied only over the depth. Energy was not conserved when A_v was updated by the Richardson number formulation explained in Section 2.3, because the internal-mode velocities would suddenly change. Presumably alterations in A_v require an expenditure of energy which is not included in the present formulation.

On the whole, the testing program has given us confidence in the numerical model and has shown the expected limits in accuracy. We now proceed to a preliminary study of the circulation in the Chesapeake Bay.

4. PROTOTYPE CHESAPEAKE BAY MODEL

One of the planned uses for the MECCA program is the simulation of salinity distributions in Chesapeake Bay during the high fresh water runoff which accompanied hurricane Agnes from June 21-27, 1972. Chesapeake Bay, the largest estuary on the U.S. coast, is broad and shallow, with dozens of major tributaries branching off the main axis (Fig. 7). The geographical complexity of the Bay prompted us to begin its study with a prototype numerical model with much simpler geometry. The complex dynamics of the Bay could then be more readily isolated and analyzed.

4.1 The Prototype Model

Early applications of the MECCA program to Chesapeake Bay showed that a model grid with 5.5 km resolution would require a large amount of computer run time. Consequently, we generated a new, prototype model grid mesh which had simpler geometry. The new grid size was 8.0 km, and had only a third of the water cells of the more detailed grid. Because of the larger grid size and fewer cells, the run time was reduced by a factor of 10.

The prototype model grid mesh for the Bay is shown in Fig. 8. Based on the bathymetry of the more detailed model, we selected a bathymetry with linearly-varying depths. At the head of the Bay, the mean sea level bay depths were on the order of 3 m, and near the mouth, 10 m. Offshore, the depth increased linearly from 10 to 22 m. The bathymetry is given in Fig. 9.

A large segment of the grid is devoted to the offshore area. Studies of the surface plume from the Bay (Ruzicki, 1981) show that the fresher water turns southward as it exits, and moves parallel to the shore down to Cape Hatteras. The outer coast boundary conditions were constructed appropriately. The deep-water boundary, parallel to shore, is assumed to act as a wall, so no flow is allowed across. Tidal flow is generally along isobaths, so the tide is applied at the northernmost open boundary perpendicular to shore. At the southernmost open perpendicular boundary, the radiation outflow condition is used.

4.2 Tidal Dynamics

The primary driving for the Bay's currents, and a major source of energy for vertical mixing, is the astronomical tide. The tide range near the mouth is

about 0.9 m, and the range first decreases then increases up the bay (National Ocean Service, 1985). The tide phase changes almost linearly with distance up the Bay.

The model was tested in the tidal mode. The initial conditions were the Bay at rest, and a uniformly decreasing salinity up the Bay. The boundary tidal input was a sinusoidal variation, with an amplitude increasing linearly up to 0.45 m after 24 h. This gradual step-up to full amplitude was necessary to suppress small-wavelength oscillations which arise when the water is subject to sudden accelerations. The tidal period was 12.0 h. We assume that the tidal currents are of first order, and that the internal mode currents due to horizontal density gradients are of second order. The salinity field was therefore kept steady for the tidal runs. The timestep was 600 s. The model was run for a simulated time of 160 h, to allow for transients to damp out. The tidal variations became quite uniform after only a few tidal cycles (Fig. 10a). The computed phase of the tide was acceptably close to the observed values (Fig. 10b), so it is not considered further.

The tide range along the axis of the Bay, based on an 80-h simulation, is shown in Fig. 12a. The relevant parameters were $C_{wb}=0.003$, $A_h=0$ m²/s, and we used no nonlinear advective terms. The range is close to that observed, except that in the lower Bay the model's results are somewhat higher. To test for model sensitivity, we varied several of the input parameters. The first case involved increasing the bottom friction coefficient from 0.003 to 0.006. The result, shown in Fig. 12b, shows a modest decrease in the tide range all along the bay. Ranges in the lower Bay are still too high.

A second test case involved adding the nonlinear advective terms to the equation. The addition of the nonlinear terms increased the run time significantly. The results are shown in Fig. 11a. The nonlinear terms have a small effect on the model's computed tide range, and we should be able to safely neglect them.

The last set of tests was for the influence of the horizontal momentum exchange coefficient, A_h . The coefficient should be in the range (Hess, 1985a)

$$0 < A_h < (\Delta L)^2/8 \Delta T = 13333 \text{ m}^2/\text{s}. \quad (51)$$

for $\Delta L=8000$ m and $\Delta T=600$ s. Three additional test cases were run, one each for $A_h=1000$, 5000, and 10,000 m²/s. The results of the model run (Figs. 12b, 13a,b) showed that increasing A_h to the first value had almost negligible effect, and increasing it to the second value modestly decreased the ranges everywhere. The third value decreased the ranges so they were too low everywhere.

These few tests showed that no simple adjustment can correct the tide range. Probably the simplified geometry accounts for the discrepancies. We decided that the tides were simulated with sufficient accuracy to proceed to the salinity tests.

4.3 Variable Salinity Computations

The next set of runs allowed for changes in salinity along with the tidal variations and with a constant river inflow. The object was to confirm that the computations are stable for a long run time. The simulated period was 10 days, and the computations were stable. The oceanic boundary conditions at the northern and southern boundaries at inflow (flow into the computational domain) appear in Fig. 14. The salinity distribution is similar to that reported by Boicourt (1973).

The salinity distribution after 10 days of computation is shown in Fig. 15. The vertical and horizontal diffusion parameters were $R_v=0.001$ and $D_h = 100$ m^2/s . We reran the model with the same boundary conditions, but with $R_v=0.100$. The isohalines, also shown in Fig. 15, show that the vertical salinity gradient is increased almost everywhere, as expected since the vertical mixing is much greater. Over a tidal cycle, the salinity value at each point fluctuated within a range of approximately 1 ppt.

The next test involved the increase of the horizontal diffusion coefficient, D_h , from $100 m^2/s$ to $1000 m^2/s$. The changes in the salinity (Fig. 16.) show up as slightly higher concentrations at all depths in the extreme upper Bay. In the lower Bay, however, the salinities at the bottom are generally lower. This is because the higher diffusion forces a more uniform distribution of isohalines. An example is the decrease in the distance between the 26- and the 31-ppt isopleths near the Bay mouth.

4.4 Hurricane Agnes

In late June 1972, hurricane Agnes meandered up the East Coast, bringing generally heavy rains to the entire Chesapeake Bay watershed (Fig. 7). Although direct rainfall was small, high volumes of fresh water entered the Bay through its many tributaries. The Susquehanna River, which normally provides about half of the river input, increased its flow by a factor of 20 over its June mean. The resulting reduction in salinity caused high mortalities of oysters, soft-shell clams, and other estuarine species.

Most of the damage to organisms occurred in the upper Bay. Soft-shell clams normally thrive in the lower-salinity water which occurs north of the Potomac River mouth. The hurricane flood, however, reduced salinities to near zero for several weeks in much of the habitat.

Along with the Susquehanna, the Potomac, Rappahannock, York, and James Rivers provide approximately 80 percent of the mean river input to the Bay. The mean daily flowrates for these rivers, as gaged by the U.S Geological Survey, for the period from 20 - 27 June, 1972 appear in Table 1.

In the months immediately following the hurricane, researchers from several of the local universities and other research institutions collected hydrographic data which quantified the changes in the Bay. These data are discussed in papers published by the U.S Army Corps of Engineers (1975a, b). There is sufficient data to warrant a model study of the event.

The hydrographic data support the following sequence of events. As massive volumes of freshwater enter the bay from the Susquehanna, the surface salinities decline, producing a low-salinity tongue which reaches as far south as the mouth of the Potomac. The upper bay is now highly stratified in terms of salinity. A few days later, the bottom salinities decline, producing a more nearly homogeneous estuary. Then, the bottom salinities rebound, overshooting the normal benthic distribution. Finally the surface salinity increases, and the bottom concentrations recede back to normal.

4.5 Model Test With Agnes Flowrates

As a final test, we ran the model for the Bay for the period 0000 local time on 21 June to 0000 local time on 12 July. The river flowrates were as shown in Table 1. For the dates 28 June to 1 July, which are not covered in the table, the Susquehanna River flowrates used were 8, 5, 3, and 2 thousands of cubic meters per second (cms). For dates after 1 July, 1.6 thousand cms was used. For the Potomac, the values for the same 4 days are 800, 500, 450, and 400 cms; thereafter 350 cms was used. The initial conditions were the currents and salinity distributions at the end of the 10-day run, for which $R_v=0.001$ and $D_h = 100 \text{ m}^2/\text{s}$.

The maximum modeled displacement of the 1-ppt and the 5-ppt isohalines occurred at the end of June 29 (day 9 in the simulation). Isopleths at the start of the simulation and at the end of day 9 are shown in Fig. 17. Salinities after 9 days throughout the Bay are lower than at the start of the run. The daily progression of the 5 ppt isohaline at the bottom down the Bay as computed by MECCA is shown in Fig. 18, along with the daily Susquehanna flow and observed isohaline displacement from its observed position on June 6-7 (Schubel, et al., 1975). The modeled displacement approximates the observed value (73 km).

The differences between the model and the observations can be due to several factors. Local depths in the model are only approximate, and the simplified grid mesh can not account for all the coastline variations. An increased diffusion value would possibly slow the rate of isohaline displacement following the peak flood by enhancing the upstream salt transport. Another possibility is that the streamflow values used in the simulation are not realistic, or that significant water entered the Bay directly over land.

5. CONCLUSIONS AND FUTURE WORK

The results from tests and simulations with MECCA show that the model can be a useful tool for describing circulations that are common to coastal areas. Tidal, wind-driven, and density-driven currents are obvious examples. MECCA can also be useful for assessing changes in salinity and temperature due to currents or unusual weather or oceanographic events.

Some features of the model can be improved. The desirability of extending the grid to cover more of the continental shelf, where the water is deeper, seems to warrant some method of grid stretching. The methods for specifying the oceanic boundary conditions should be studied further.

6. REFERENCES

- Bishop, J. M., and J. E. Overland, 1977: Seasonal drift on the middle Atlantic shelf. Deep-Sea Res., 24, 161-169.
- Blumberg, A. F., and G. L. Mellor, 1981: A Numerical Calculation of the Circulation in the Gulf of Mexico. Dynalysis of Princeton Report no. 66., Princeton, N.J., 153 pp.
- Boicourt, W., 1973: The circulation of water on the continental shelf from Chesapeake Bay to Cape Hatteras. Ph. D. thesis, Johns Hopkins University, Baltimore Md., pp 183.
- Bryan, K., 1975: Three-Dimensional Numerical Models of the Ocean Circulation. Numerical Models of Ocean Circulation, National Academy of Sciences, Washington, DC, 94-106.
- Crank, J., 1956: The Mathematics of Diffusion. Oxford, London, 347 pp.
- Ekman, V. W., 1905: On the influence of the earth's rotation on ocean-currents. Ark. Mat. Ast. Fys., 2, 1-53.
- Hess, K. W., 1976: A three-dimensional numerical model of the estuary circulation and salinity in Narragansett Bay. Est. Coast. Mar. Sci., 4, 325-338.
- _____, 1985a: A finite-difference scheme for vertically-integrated horizontal flows. MEAD Office Note 85-1, National Environmental Satellite, Data, and Information Service, NOAA, U.S. Department of Commerce, 17 pp. (available from: Chief, Marine Environmental Assessment Division, Assessment and Information Services Center, NESDIS, Washington, DC 20235)
- _____, 1985b: Numerical solution for the internal-mode velocities. MEAD Office Note 85-2, National Environmental Satellite, Data, and Information Service, NOAA, U.S. Department of Commerce, 12 pp. (available from: Chief, Marine Environmental Assessment Division, Assessment and Information Services Center, NESDIS, Washington, DC 20235)
- _____, 1985c: Numerical solution of the three-dimensional concentration equation. MEAD Office Note 85-3, National Environmental Satellite, Data, and Information Service, NOAA, U.S. Department of Commerce, 8 pp. (available from: Chief, Marine Environmental Assessment Division, Assessment and Information Services Center, NESDIS, Washington, DC 20235)
- _____, and F. M. White, 1974: A numerical tidal model of Narragansett Bay, University of Rhode Island Marine Tech. Report 20, pp 141.
- Ippen, A. T., and D. R. F. Harleman, 1966: Tidal dynamics in estuaries. Estuary and Coastline Hydrodynamics, A. T. Ippen, ed., 493-545.
- Liu, S.-K., and J. J. Leendertse, 1978: Multidimensional Numerical Modeling of Estuaries and Coastal Seas. Advances in Hydroscience, 11, 95-164.
- National Ocean Service, 1985: Tide Tables: East coast of North and South America.

- Ramming, H.-G., and Z. Kowalik, 1980: Numerical Modelling of Marine Hydrodynamics. Elsevier, New York, pp 368.
- Ruzecki, E. P., 1981: Temporal and spatial variations of the Chesapeake Bay plume. Chesapeake Bay Plume Study: Superflux 1980 (J. W. Campbell and J. P. Thomas, eds.), NASA Conference Publication 2188, 111-130.
- Schubel, J. R., H. H. Carter, and W. B. Cronin, 1975: Effects of Agnes on the distribution of salinity along the main axis of the Bay, and in contiguous shelf waters. In "Impact of Tropical Storm Agnes on Chesapeake Bay: Appendix (J. Davis, ed.), U.S. Army Corps of Engineers, Baltimore District, A1- A38.
- Sheng, Y. P., 1983: Mathematical Modeling of Three-Dimensional Coastal Currents and Sediment Dispersion: Model Development and Application. U.S. Army Corps of Engineers Tech. Report CERC-83-2, Washington DC, pp 288.
- U.S. Army, 1975a: Impact of tropical storm Agnes on Chesapeake Bay: Summary, Corps of Engineers, Baltimore District, pp 46 + plates.
- _____, 1975b: Impact of tropical storm Agnes on Chesapeake Bay: Appendix, Corps of Engineers, Baltimore District, pp 51 + appendices.
- Wu, J. 1975: Wind-stress coefficients over sea surface near neutral conditions - a revisit. J. Phys. Oceanog., 10, 727-740.
- Wurtele, M. G., J. Paegle, and A. Sielecki, 1971: The use of open boundary conditions with the storm-surge equations. Mon. Wea. Rev., 99, 537-544.

APPENDIX I. List of Symbols

- A_h = horizontal momentum exchange coefficient,
 A_v = vertical momentum exchange coefficient,
 b = factor for velocity deviations from the mean,
 c = salinity (ppt),
 C = depth-integrated concentration,
 C^* = an integral of concentration over depth,
 d = water depth at mean sea level,
 D_h = horizontal mass exchange coefficient,
 D_v = vertical mass exchange coefficient,
 f = Coriolis acceleration = $2 \sin(\text{latitude})$,
 g = gravitational acceleration,
 h = water level above mean sea level,
 H = total water depth,
 k = von Karman's constant,
 p = fluid pressure,
 p_a = atmospheric pressure at the sea surface,
 P^* = horizontal pressure gradient due to variable density,
 q = dimensionless vertical coordinate,
 r = ratio of air and water density,
 t = time,
 $T_{sx, sy}$ = wind stress per unit water density on water surface in x-, y-directions,
 $T_{bx, by}$ = bottom stress per unit water density on water in x-, y-directions,
 u, v, w = total velocity components in x-, y-, and z-directions,
 U, V = depth-integrated flowrates per unit width in x-, y-directions,
 u', v' = internal mode velocities (departures from vertical average),
 u'', v'' = depth-averaged velocities in x-, y-direction.
 V_{10} = wind speed at 10 meters,
 V_x, V_y = components of wind in x-, y-directions,
 x, y, z = axial directions in the Cartesian coordinate system,
 = density enhancement factor per unit salinity,
 = water density,
 ρ = reference density, and
 ω = earth's rotation rate.

APPENDIX II. The Model Equations

1. The Basic Equations for Shallow-water Circulation.

The equations for a fluid in a rotating orthogonal reference frame with the z-axis directed upward, are applied to the coastal region. We use the mathematical convention and denote a partial derivative of a variable with respect to a parameter as that variable followed by a subscript comma and the parameter. Two parameters in the subscript denote multiple differentiation. The x- and y-momentum equations (Bryan, 1975) are

$$u_{,t} + (uu)_{,x} + (uv)_{,y} + (uw)_{,z} = -1/\rho_0 p_{,x} + fv + A_h(u_{,xx} + u_{,yy}) + (A_v u_{,z})_{,z} \quad (\text{A.1})$$

and

$$v_{,t} + (vu)_{,x} + (vv)_{,y} + (vw)_{,z} = -1/\rho_0 p_{,y} - fu + A_h(v_{,xx} + v_{,yy}) + (A_v v_{,z})_{,z}. \quad (\text{A.2})$$

The hydrostatic equation is

$$p_{,z} = -\rho g. \quad (\text{A.3})$$

The equation for mass conservation is

$$u_{,x} + v_{,y} + w_{,z} = 0. \quad (\text{A.4})$$

The equation of state is

$$\rho = \rho_0(1 + \alpha c). \quad (\text{A.5})$$

The conservation of concentration (mass of solute per mass sea water) is

$$c_{,t} + (uc)_{,x} + (vc)_{,y} + (wc)_{,z} - D_h(c_{,xx} + c_{,yy}) - (D_v c_{,z})_{,z} = 0. \quad (\text{A.6})$$

Values of the parameters are $g = 9.81 \text{ m/s}^2$, $\rho_0 = 1 \text{ gm/cm}^3$, and $\alpha = 0.0008 \text{ ppt}^{-1}$. Here $f = 2\Omega \sin(\text{latitude})$, where $\Omega = 0.0000729 \text{ s}^{-1}$.

2. The Vertically-Integrated Momentum Equations.

A tremendous savings in computer time is achieved if the internal, or baroclinic, mode of flow is separated from the external, or barotropic, mode. To accomplish this we must integrate the equations over the vertical. First, we get an expression for the pressure by integrating the hydrostatic equation from the bottom, $z=-d$, to the top, $z=h$, of the water column. Thus

$$p = p_a - \int_h^z \rho g dz = p_a - \rho_0 g(z - h) - \alpha g \int_h^z c dz \quad (\text{A.7})$$

where p_a is the atmospheric pressure at the sea surface.

The horizontal momentum equations are then integrated over the vertical to yield

$$U_{,t} + b[(UU/H)_{,x} + (UV/H)_{,y}] = -gH h_{,x} - P^*_{,x} + fV + T_{sx} - T_{bx} + A_h[U_{,xx} + U_{,yy}] + \text{HOT}, \quad (\text{A.8})$$

and

$$V_{,t} + b[(VU/H)_{,x} + (VV/H)_{,y}] = -gH h_{,y} - P^*_{,y} - fU + T_{sy} - T_{by} + A_h[V_{,xx} + V_{,yy}] + \text{HOT}, \quad (\text{A.9})$$

and the integrated mass equation becomes

$$h_{,t} + U_{,x} + V_{,y} = 0, \quad (\text{A.10})$$

where HOT are higher-order terms arising from the integration of the horizontal diffusion terms and the non-linear advective terms since b is not truly constant. These terms will be neglected. Also,

$$(U, V, C) = \int_{-d}^h (u, v, c/H) dz,$$

$$H = h + d,$$

$$P^*_r = (p_a)_{,r} - (\alpha g/2)(C^*H^2)_{,r} - \alpha gH C d_{,r} \quad (r=x \text{ or } y),$$

$$C^* = H^{-2} \int_h^{-d} \int_h^z c \, dr dz,$$

In the derivation of the integrated equations, we have used Leibnitz's rule to bring the derivatives outside the integral. Also, we have used the kinematic boundary conditions, which are

$$w = dh/dt = h_{,t} + uh_{,x} + vh_{,y} \quad \text{at } z = h,$$

and

$$w = 0 = -ud_{,x} - vd_{,y} \quad \text{at } z = -d.$$

3. Equations for Mean Horizontal Velocities

It will become apparent in the next section that the momentum equations will be more convenient if they are recast as expressions for the mean velocities, which are defined as

$$u'' = U/H \quad \text{and} \quad v'' = V/H.$$

The recast horizontal momentum equations then become

$$u''_{,t} + b[u''u''_{,x} + v''u''_{,y}] = -gh_{,x} - P^*_x/H + fv'' + (T_{sx} - T_{bx})/H + (A_h/H)[(u''H)_{,xx} + (u''H)_{,yy}] \quad (A.11)$$

and

$$v''_{,t} + b[u''v''_{,x} + v''v''_{,y}] = -gh_{,y} - P^*_y/H - fu'' + (T_{sy} - T_{by})/H + (A_h/H)[(v''H)_{,xx} + (v''H)_{,yy}]. \quad (A.12)$$

4. The Internal Mode Equations

The internal mode horizontal velocities are defined as

$$u' = u - u'' \quad \text{and} \quad v' = v - v''.$$

The equations of internal mode motion are derived by subtracting the external mode equations for the mean velocities from the total equation to get

$$u'_{,t} + uu'_{,x} + u'u''_{,x} + vu'_{,y} + v'u''_{,y} + wu'_{,z} = fv' + \alpha g \left(\int_h^z cdz \right)_{,x} + P^*_x - (T_{sx} - T_{bx})/H + (A_v u'_{,z})_{,z} + A_h [u'_{,xx} + u'_{,yy} - (u''/H)(H_{,xx} + H_{,yy})] \quad (A.13)$$

and

$$v'_{,t} + uv'_{,x} + u'v''_{,x} + vv'_{,y} + v'v''_{,y} + wv'_{,z} = -fu' + \alpha g \left(\int_h^z cdz \right)_{,y} + P^*_y - (T_{sy} - T_{by})/H + (A_v v'_{,z})_{,z} + A_h [v'_{,xx} + v'_{,yy} - (v''/H)(H_{,xx} + H_{,yy})] \quad (A.14)$$

The last term in each of (A.13) and (A.14), which contains the Laplacian of the total depth, will be neglected.

5. The Dimensionless Vertical Coordinate

We have chosen to recast the equations with the use of a dimensionless vertical coordinate. This permits the use of a constant number of vertical levels at all grids. The new coordinate is

$$q = (z - h)/H,$$

and has the value of 0 at the water surface, and -1 at the bottom. Partial derivatives with respect to z of a variable in the x, y, z, t -coordinate system, [], are transformed to derivatives of the same variable in the x, y, q, t -coordinate system, () by substituting

$$[]_{,z} = H^{-1} ()_{,q}$$

and with respect to the horizontal variable r ($= x$ or y) by substituting

$$[]_{,r} = ()_{,r} - [H^{-1}(h_{,r} + qH_{,r})]()_{,q}$$

and with respect to time by

$$[]_{,t} = ()_{,t} - [H^{-1}(1+q)h_{,t}]()_{,q}$$

The vertical velocity in the new coordinate system is

$$\begin{aligned} w = dz/dt &= d/dt(Hq + h) = (Hq + h)_{,t} + u(Hq + h)_{,x} + v(Hq + h)_{,y} \\ &= HQ + (1 + q)h_{,t} + u(h_{,x} + qH_{,x}) + v(h_{,y} + qH_{,y}) \end{aligned} \quad (A.15)$$

where $Q = q_{,t}$.

The momentum equations in the new coordinate system become

$$\begin{aligned} u'_{,t} + uu'_{,x} + u'u''_{,x} + vv'_{,y} + v'u''_{,y} + Qu'_{,q} &= fv' + P_x^*/H \\ + \alpha g[(H \int_0^q cdq)_{,x} - (h_{,x} + qH_{,x})c] + H^{-2}(A_v u'_{,q})_{,q} \\ - (T_{sx} - T_{bx})/H + A_h[u'_{,xx} + u'_{,yy}] + \text{HOT}, \end{aligned} \quad (A.17)$$

and

$$\begin{aligned} v'_{,t} + uv'_{,x} + u'v''_{,x} + vv'_{,y} + v'v''_{,y} + Qv'_{,q} &= -fu' + P_y^*/H \\ + \alpha g[(H \int_0^q cdq)_{,y} - (h_{,y} + qH_{,y})c] + H^{-2}(A_v v'_{,q})_{,q} \\ - (T_{sy} - T_{by})/H + A_h[v'_{,xx} + v'_{,yy}] + \text{HOT}, \end{aligned} \quad (A.18)$$

where HOT are higher-order horizontal diffusion terms arising from the fact that u' and v' vary over q . These terms will be neglected. The continuity equation becomes

$$(Hu')_{,x} + (Hv')_{,y} + HQ_{,q} = 0, \quad (A.19)$$

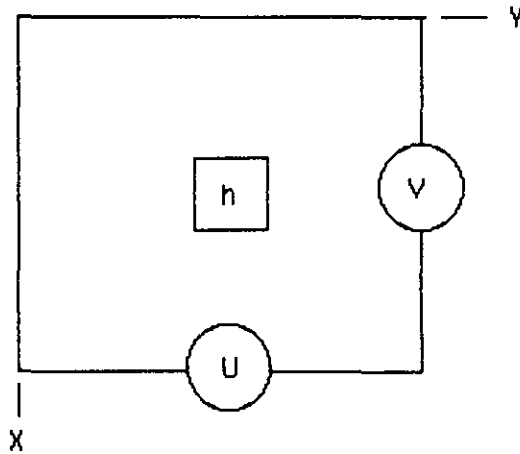
and the concentration equation is

$$\begin{aligned} (Hc)_{,t} + (Huc)_{,x} + (Hvc)_{,y} + (HQc)_{,q} - H^{-1}(D_v c)_{,q} \\ - HD_h[c_{,xx} + c_{,yy}] = 0. \end{aligned} \quad (A.20)$$

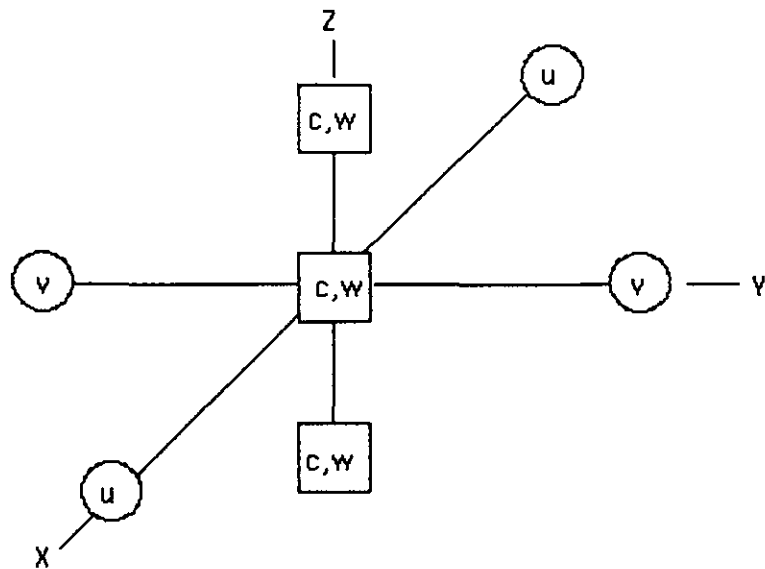
The system of equations is now complete.

Table 1. Daily mean river flowrates during the passage of hurricane Agnes (U.S. Army, 1975a). Units are m^3/s . (' = peak value for day rather than mean)

River	June Date							
	20	21	22	23	24	25	26	27
Susquehanna	1534	1426	12593	29432	31979'	28583	19696	11829
Potomac	203	340	4868	7584	10159'	5660	2258	1007
Rappahannock	31	181	3028'	1259	515	210	144	130
York	51	88	296	1008'	971	940	812	608
James	261	405	3849	8858'	5943	2510	812	563



(a) TOP VIEW - EXTERNAL MODE VARIABLES



(b) ISOMETRIC VIEW - INTERNAL MODE VARIABLES

Figure 1. Placement on variables of the grid mesh. (a) Top view showing the external-mode variables. (b) Isometric view showing the internal-mode velocities, the vertical velocities, and the concentration.

RECTANGULAR TEST BASIN

— ANALYTIC — MECCA

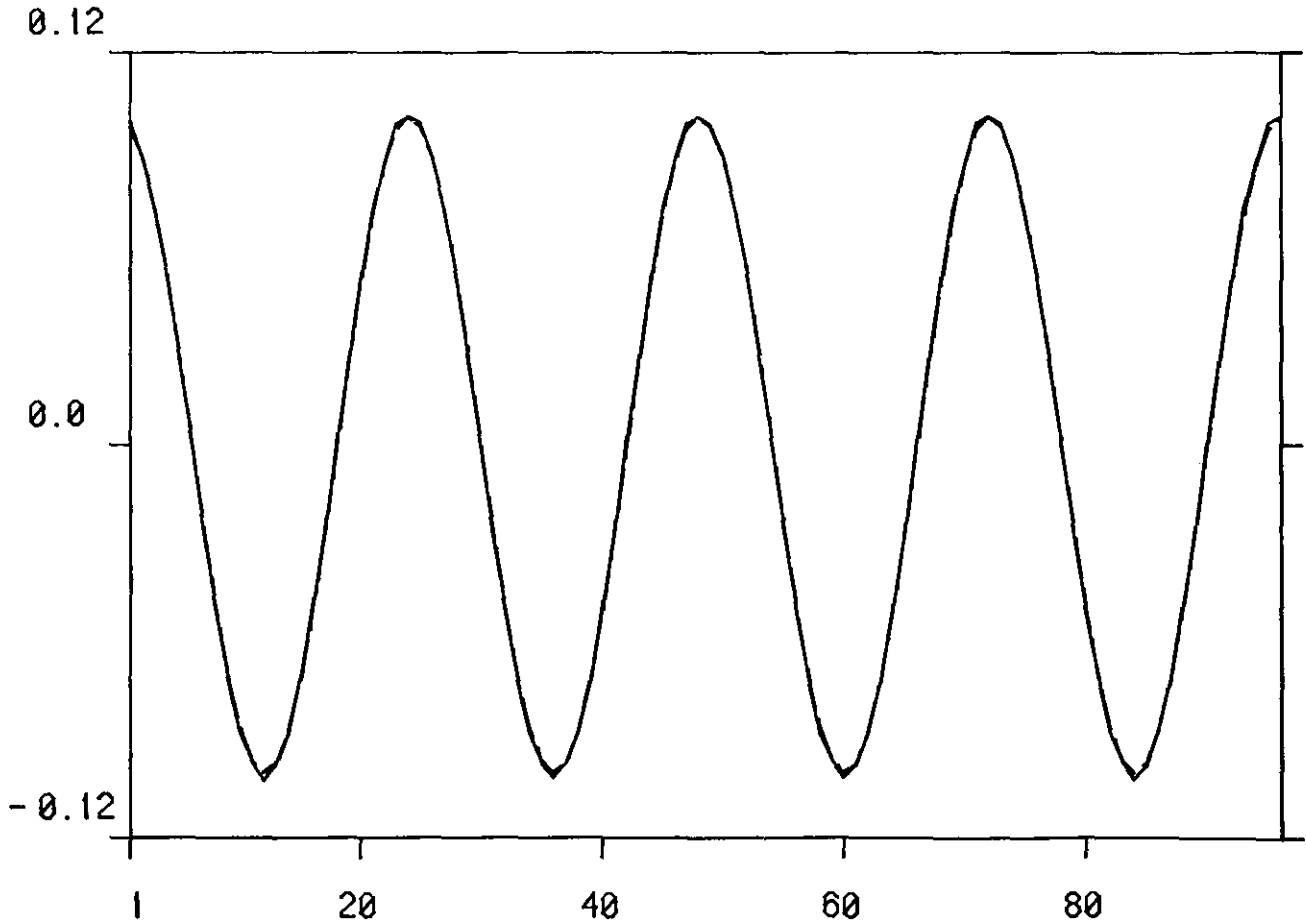


Figure 2. Comparison of computed and analytic water levels for the case of the forced oscillation at the open end of a rectangular basin of uniform depth. The MECCA solution is nearly identical to the analytic solution. The vertical scale has units of meters, and the horizontal scale units are timesteps (one timestep equals 30 minutes).

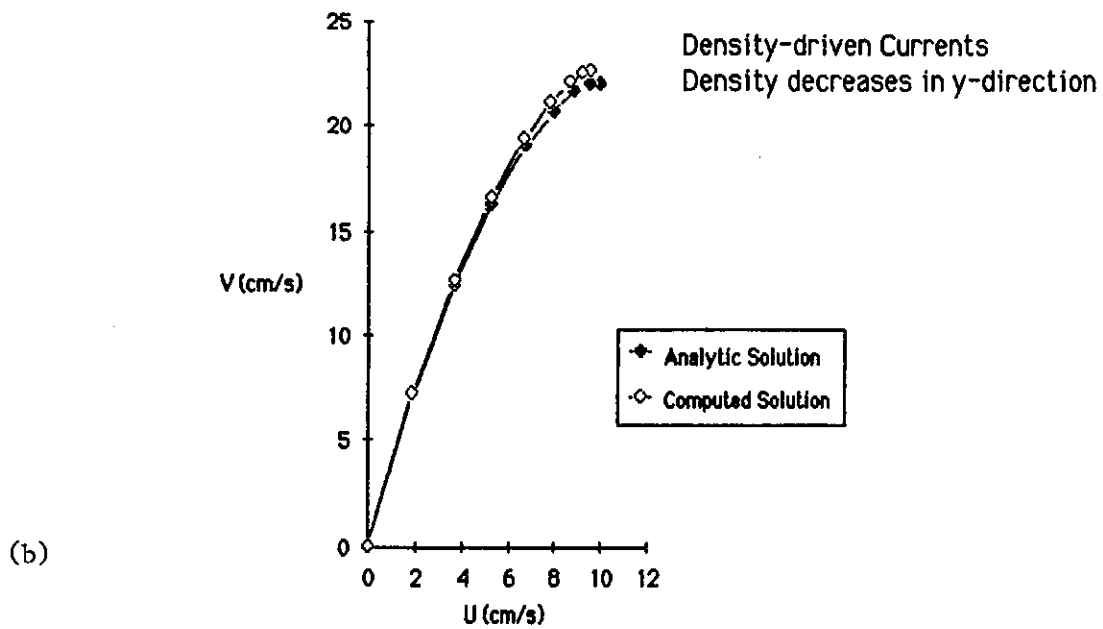
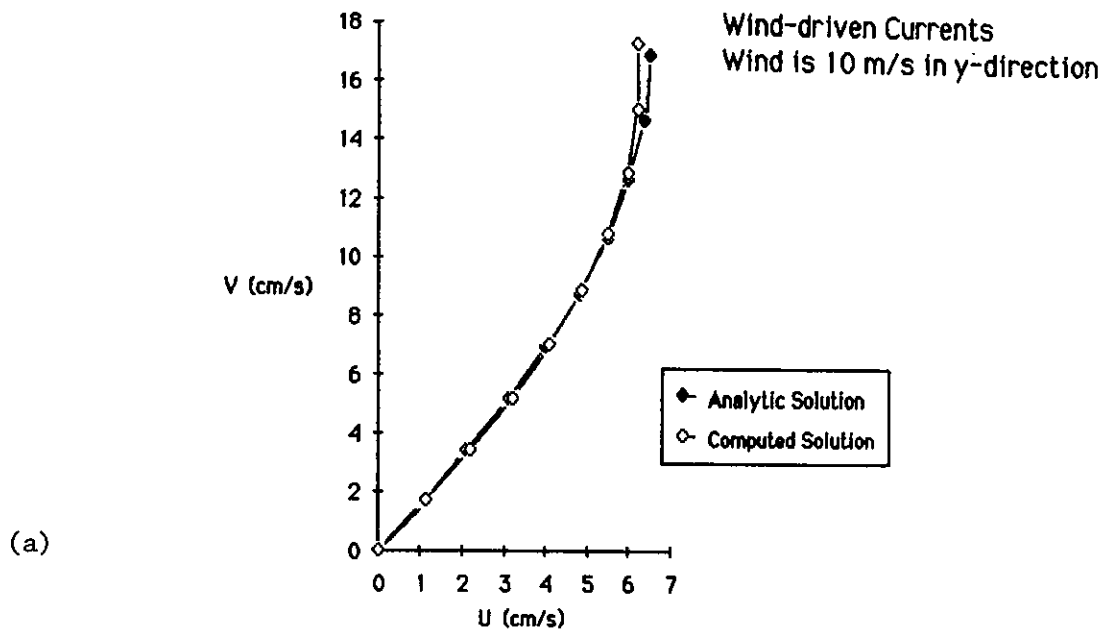


Figure 3. (a) Comparison of computed and analytic wind-driven currents. (b) Comparison of computed and analytic density-driven currents.

Non-linear Velocity Advection Balanced by Bottom Friction

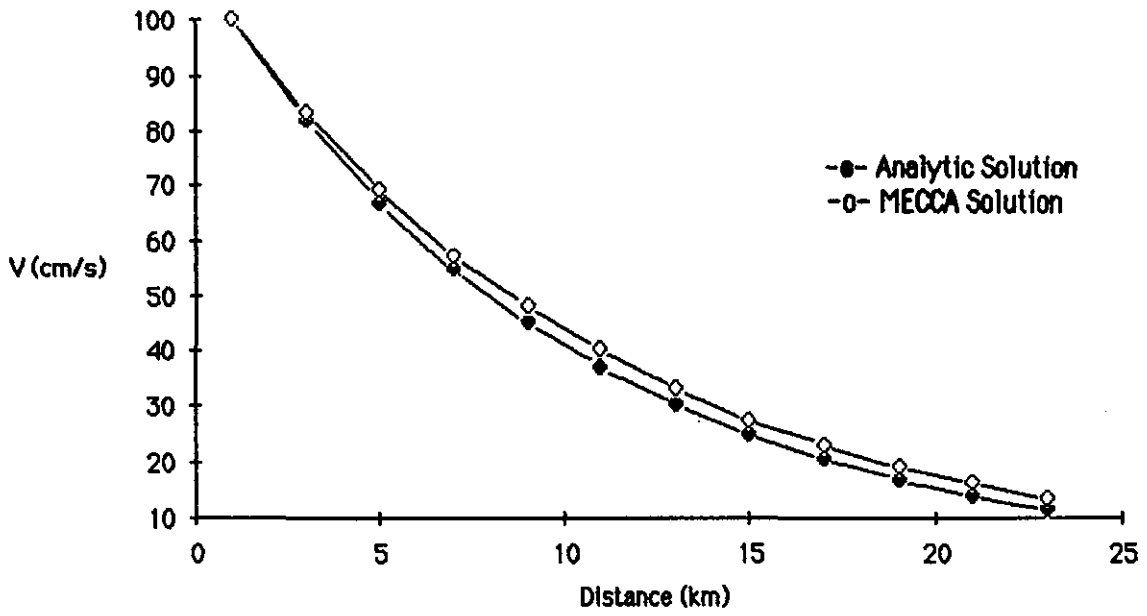


Figure 4. Comparison of computed and analytic velocities for the test of the non-linear advection terms in the momentum equation.

HORIZONTAL DIFFUSION

$D_h = 1000 \text{ m}^2/\text{s}$

— Analytic Solution
-- MECCA Solution

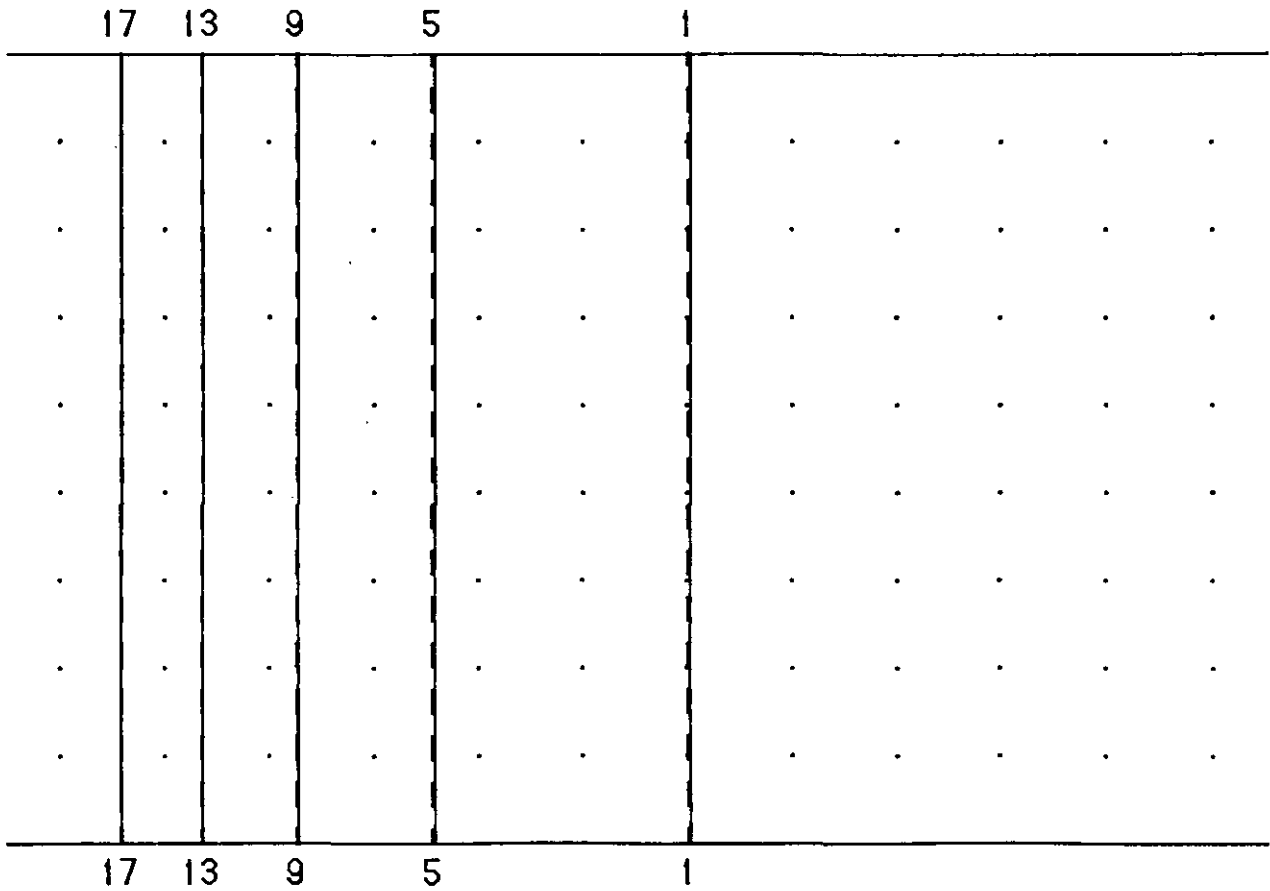


Figure 5. Comparison of computed and analytic concentration distribution for the case of pure horizontal diffusion after 32 hours. Basin depth is 10 m, and basin length shown is 55 km.

HORIZONTAL ADVECTION AND VERTICAL DIFFUSION

— Analytic Solution
-- MECCA Solution

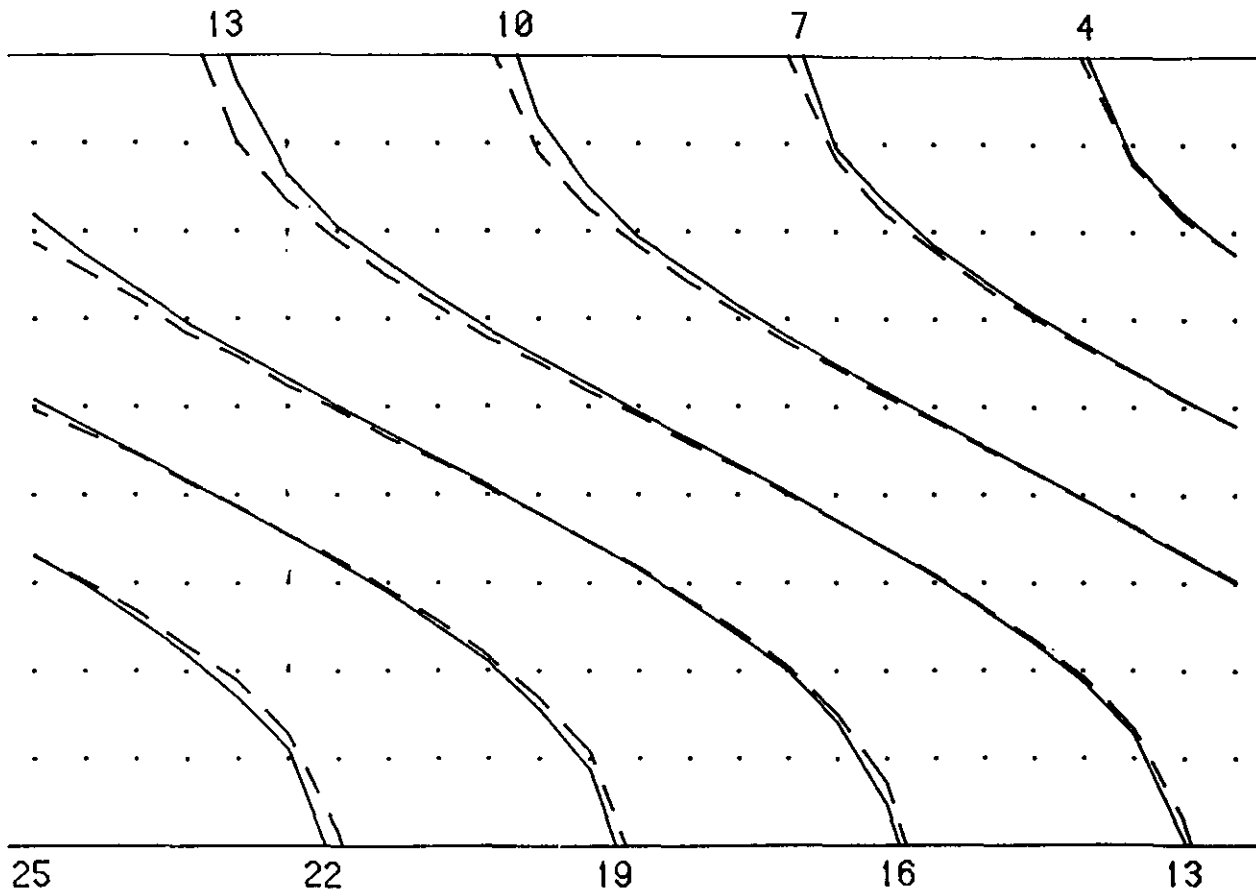


Figure 6. Comparison of computed and analytic concentration distribution for the case of horizontal advection balanced by vertical diffusion. Basin depth is 20 m, and total basin length is 120 km.

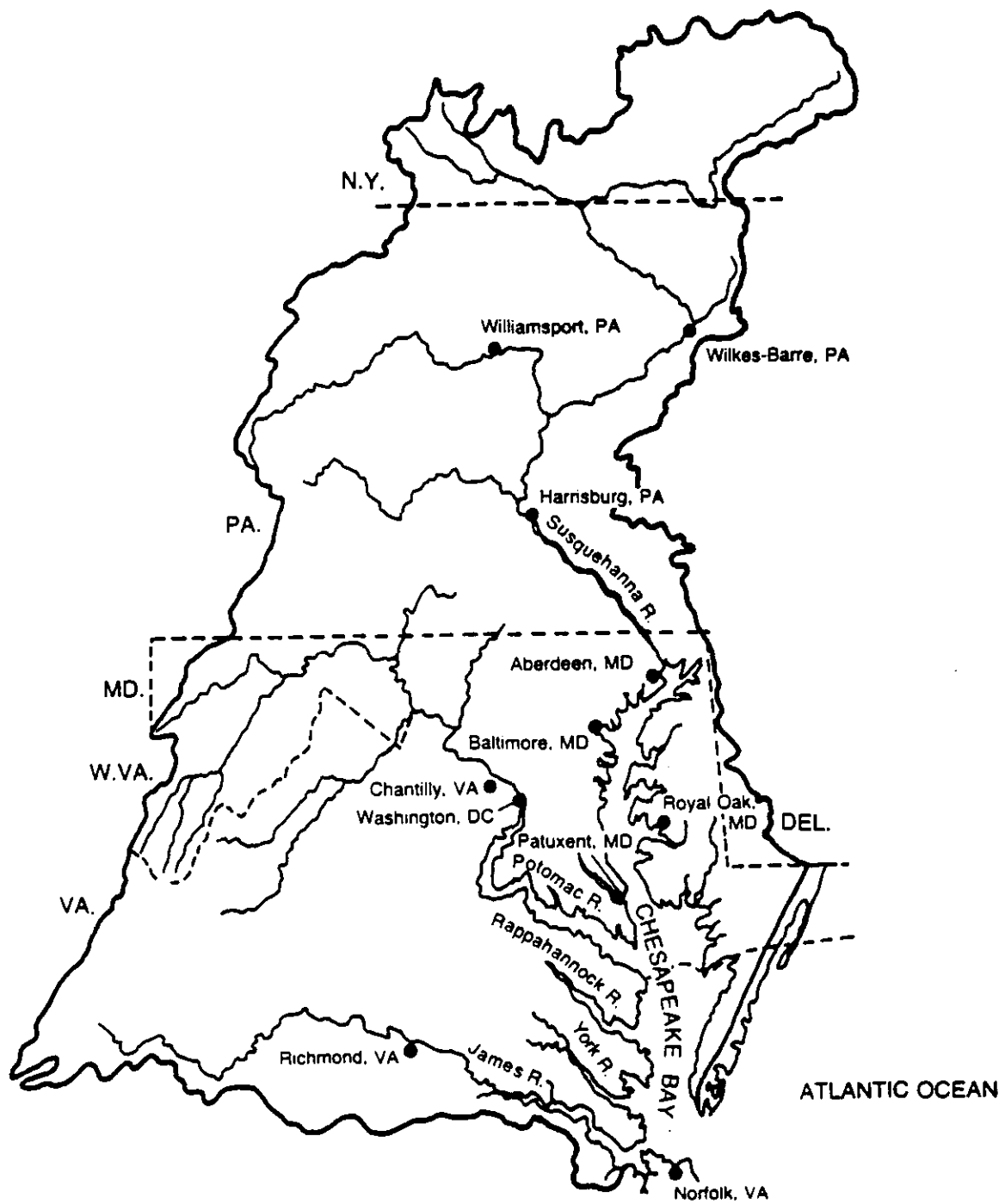


Figure 7. Chesapeake Bay watershed. Major rivers are the Susquehanna, Potomac, Rappahannock, York, and James.

PROTOTYPE CHESAPEAKE BAY GRID MESH
 $\Delta L = 8.0 \text{ KM}$

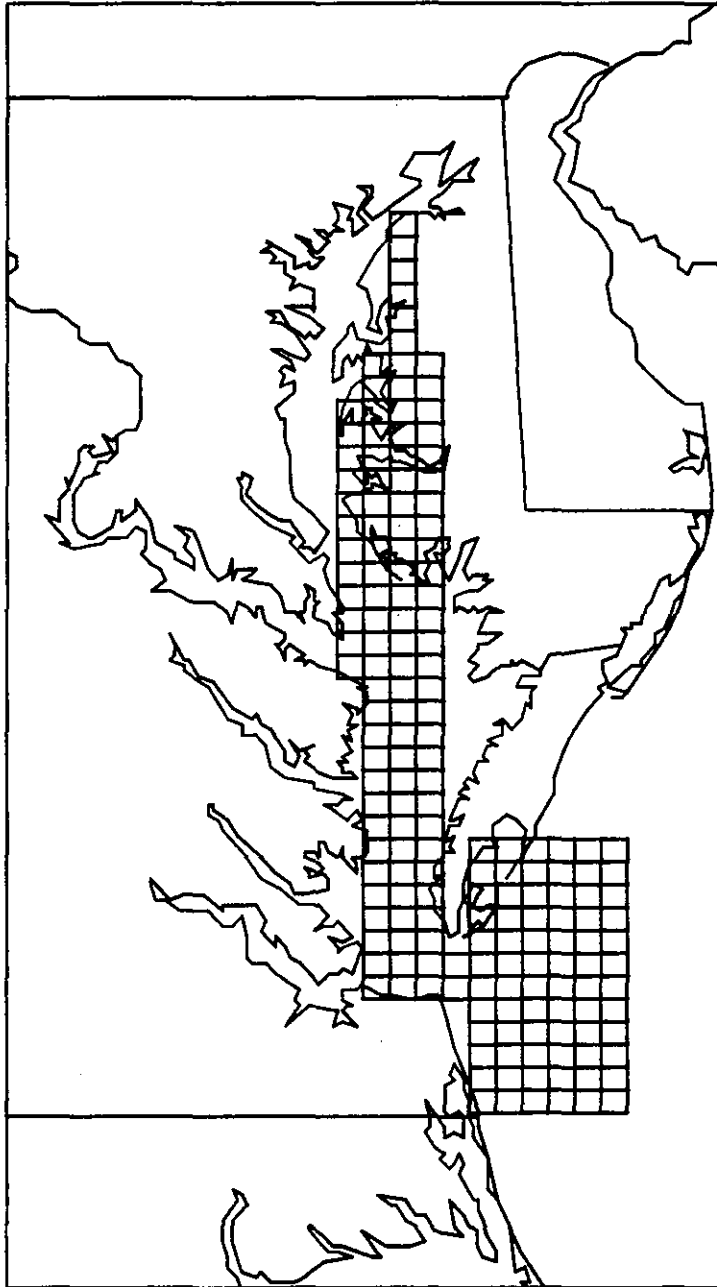


Figure 8. Grid mesh for the prototype model for Chesapeake Bay. The mesh consists of 176 cells, with a spacing of 8 km.

PROTOTYPE CHESAPEAKE BAY GRID DEPTHS (M)

DEPTHS (M) AT MSL

	1	2	3	4	5	6	7	8	9	10	11	12
1	0	0	0	0	0	0	0	0	0	0	0	0
2	0	0	0	3	0	0	0	0	0	0	0	0
3	0	0	0	3	0	0	0	0	0	0	0	0
4	0	0	0	3	0	0	0	0	0	0	0	0
5	0	0	0	3	0	0	0	0	0	0	0	0
6	0	0	0	3	0	0	0	0	0	0	0	0
7	0	0	0	4	0	0	0	0	0	0	0	0
8	0	0	4	4	4	0	0	0	0	0	0	0
9	0	0	4	4	4	0	0	0	0	0	0	0
10	0	4	4	4	4	0	0	0	0	0	0	0
11	0	4	4	4	4	0	0	0	0	0	0	0
12	0	5	5	5	5	0	0	0	0	0	0	0
13	0	5	5	5	5	0	0	0	0	0	0	0
14	0	5	5	5	5	0	0	0	0	0	0	0
15	0	5	5	5	5	0	0	0	0	0	0	0
16	0	6	6	6	6	0	0	0	0	0	0	0
17	0	6	6	6	6	0	0	0	0	0	0	0
18	0	6	6	6	6	0	0	0	0	0	0	0
19	0	6	6	6	6	0	0	0	0	0	0	0
20	0	6	6	6	6	0	0	0	0	0	0	0
21	0	7	7	7	7	0	0	0	0	0	0	0
22	0	0	7	7	7	0	0	0	0	0	0	0
23	0	0	7	7	7	0	0	0	0	0	0	0
24	0	0	7	7	7	0	0	0	0	0	0	0
25	0	0	8	8	8	0	0	0	0	0	0	0
26	0	0	8	8	8	0	0	0	0	0	0	0
27	0	0	8	8	8	0	0	0	0	0	0	0
28	0	0	8	8	8	0	10	13	16	19	22	22
29	0	0	8	8	8	0	10	13	16	19	22	22
30	0	0	9	9	9	0	10	13	16	19	22	22
31	0	0	9	9	9	0	10	13	16	19	22	22
32	0	0	9	9	9	0	10	13	16	19	22	22
33	0	0	9	9	9	0	10	13	16	19	22	22
34	0	0	10	10	10	10	10	13	16	19	22	22
35	0	0	10	10	10	10	10	13	16	19	22	22
36	0	0	0	0	0	0	10	13	16	19	22	22
37	0	0	0	0	0	0	10	13	16	19	22	22
38	0	0	0	0	0	0	10	13	16	19	22	22
39	0	0	0	0	0	0	10	13	16	19	22	22
40	0	0	0	0	0	0	10	13	16	19	22	22

Figure 9. Depths (m) for the water grids in the prototype Chesapeake Bay model grid.

CHESAPEAKE BAY PROTOTYPE MODEL

COMPUTED TIDES (M) AT THREE LOCATIONS

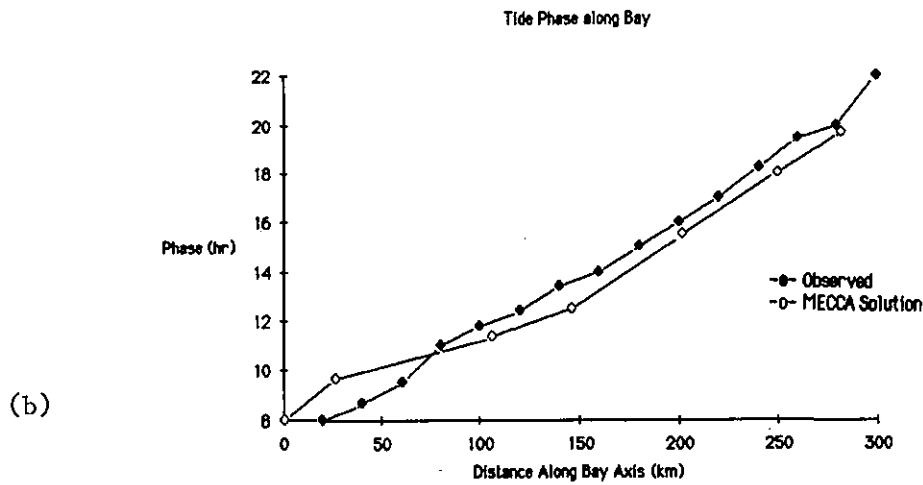
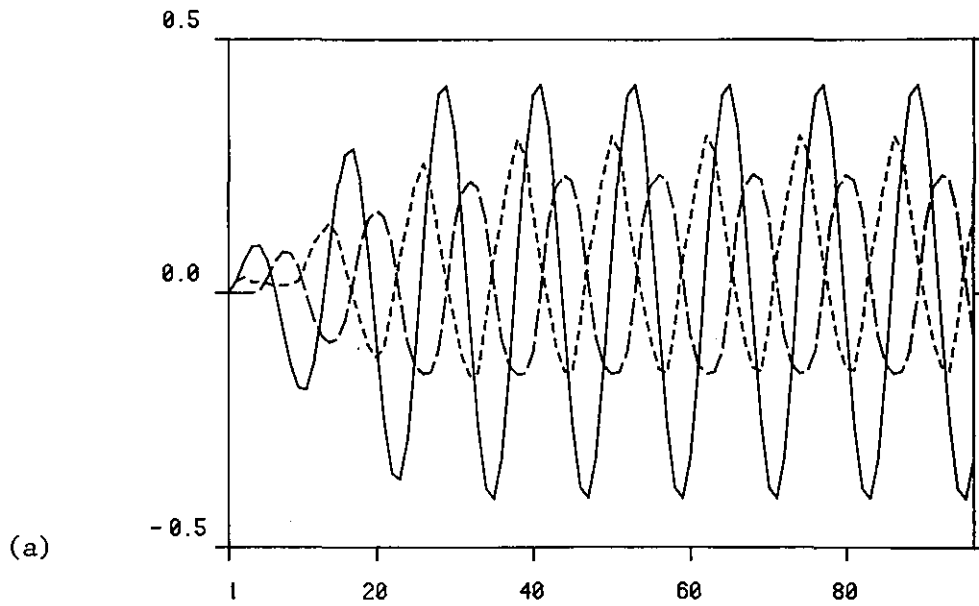
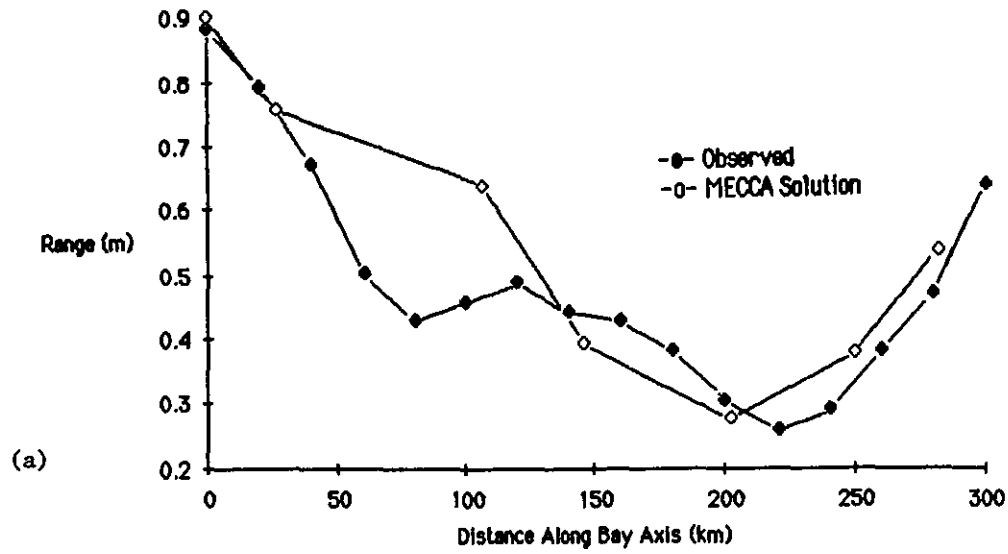


Figure 10. (a) Tide heights (meters) at three points in the prototype grid. Horizontal units are hours. Transients damp out after a few cycles. (b) Comparison of observed and computed tide phases for $C_{wb}=0.003$.

Tide Range Along Bay - $C_{wb} = 0.003$



Tide Range along Bay - $C_{wb} = 0.006$

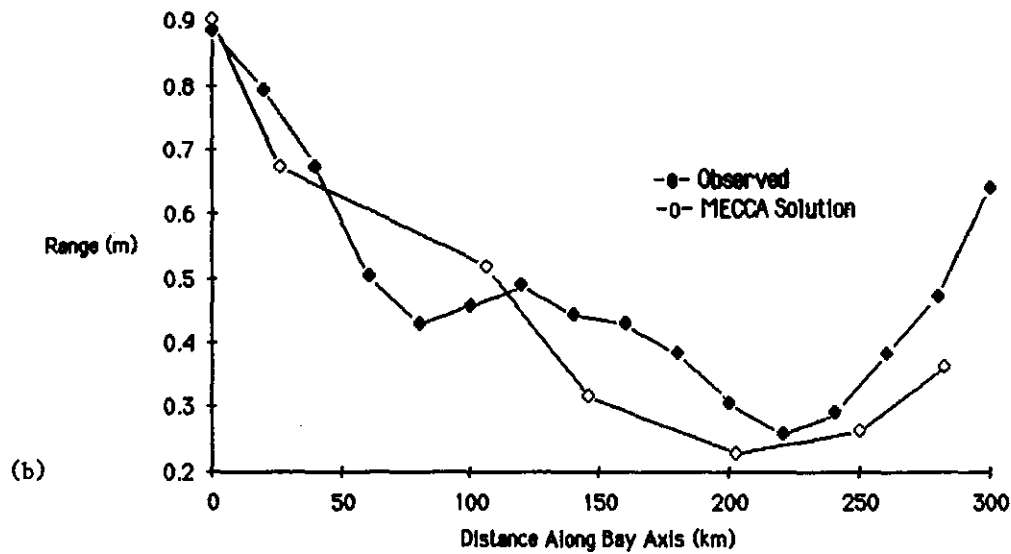
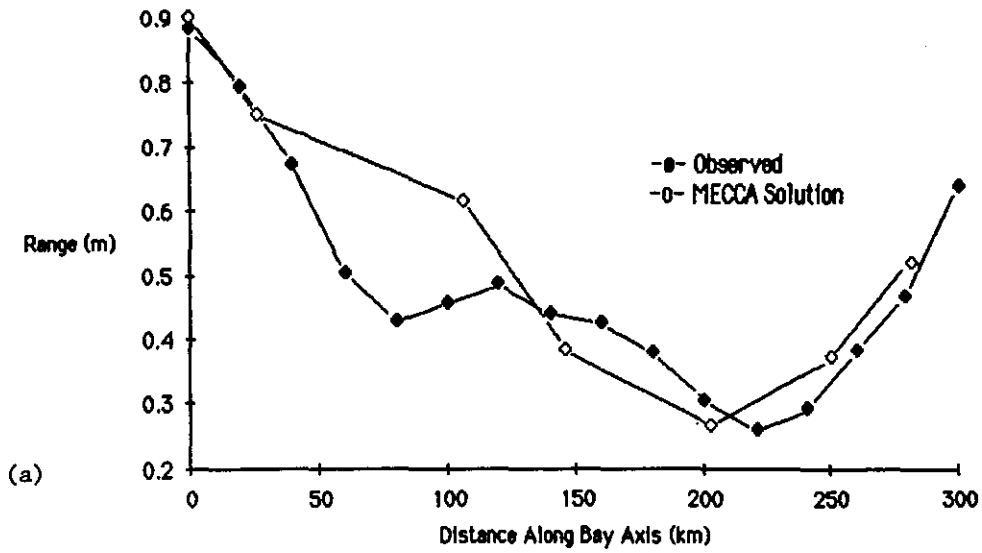


Figure 11. (a) Comparison of observed and computed mean tide ranges along the Bay. $C_{wb}=0.003$. (b) Comparison for $C_{wb}=0.006$.

Tide Range Along Bay with Non-linear Advection



Tide Range along Bay with $A=1000$

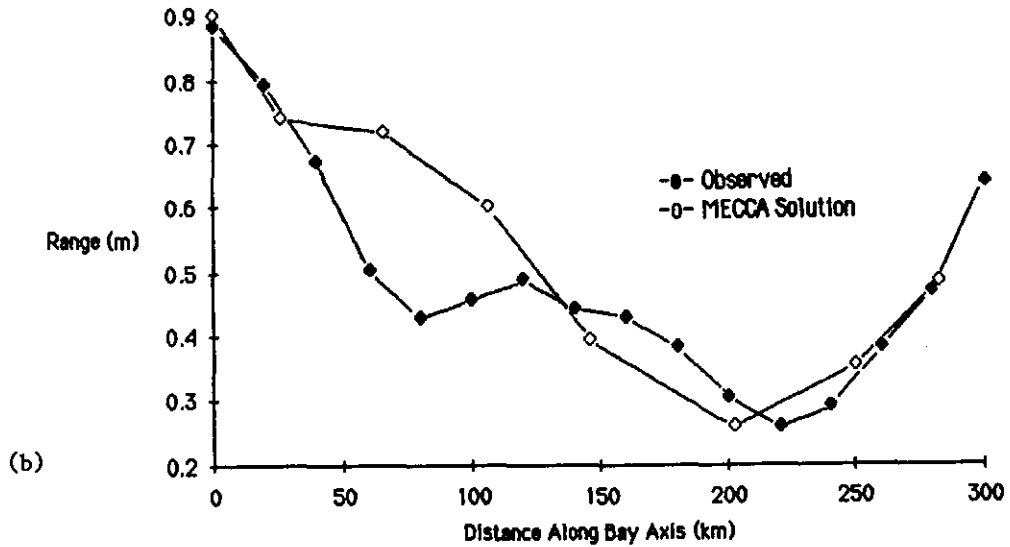
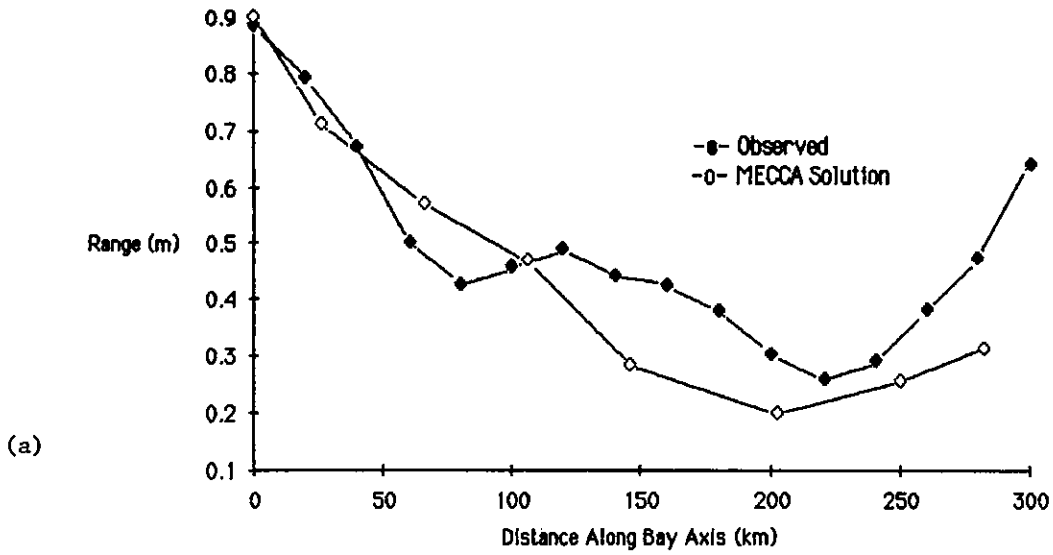


Figure 12. (a) Same as Fig. 11a, but with the non-linear terms. (b) Same as Fig 12a, but with $A_h = 1000 \text{ m}^2/\text{s}$.

Tide Range along Bay with A=5000



Tide Range along Bay with A=10,000

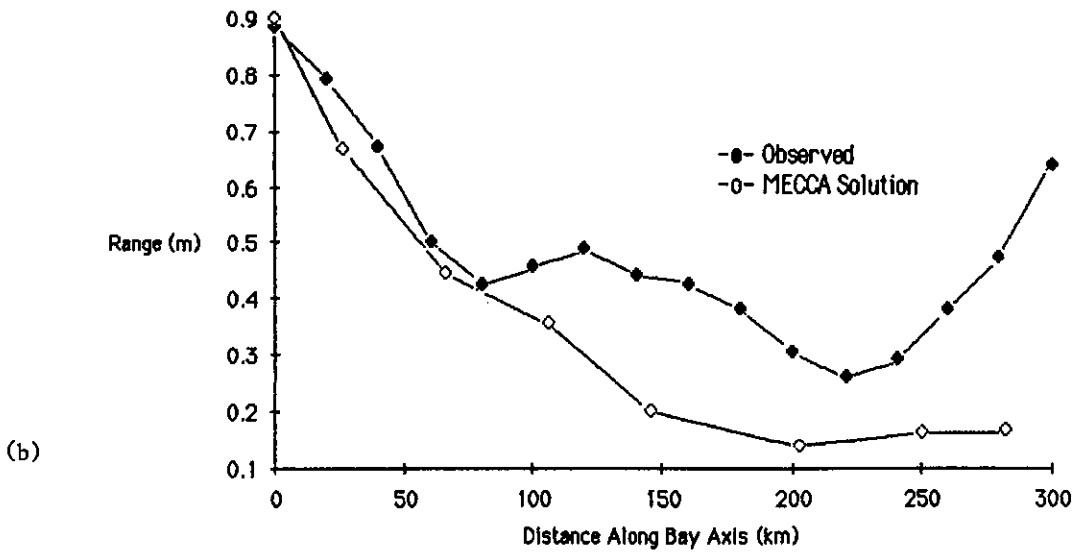


Figure 13. (a) Same as Fig. 11a, but with $A_h=5000 \text{ m}^2/\text{s}$. (b) Same as Fig. 12a, but with $A_h=10,000 \text{ m}^2/\text{s}$.

CHESAPEAKE BAY PROTOTYPE MODEL
LOOKING NORTH

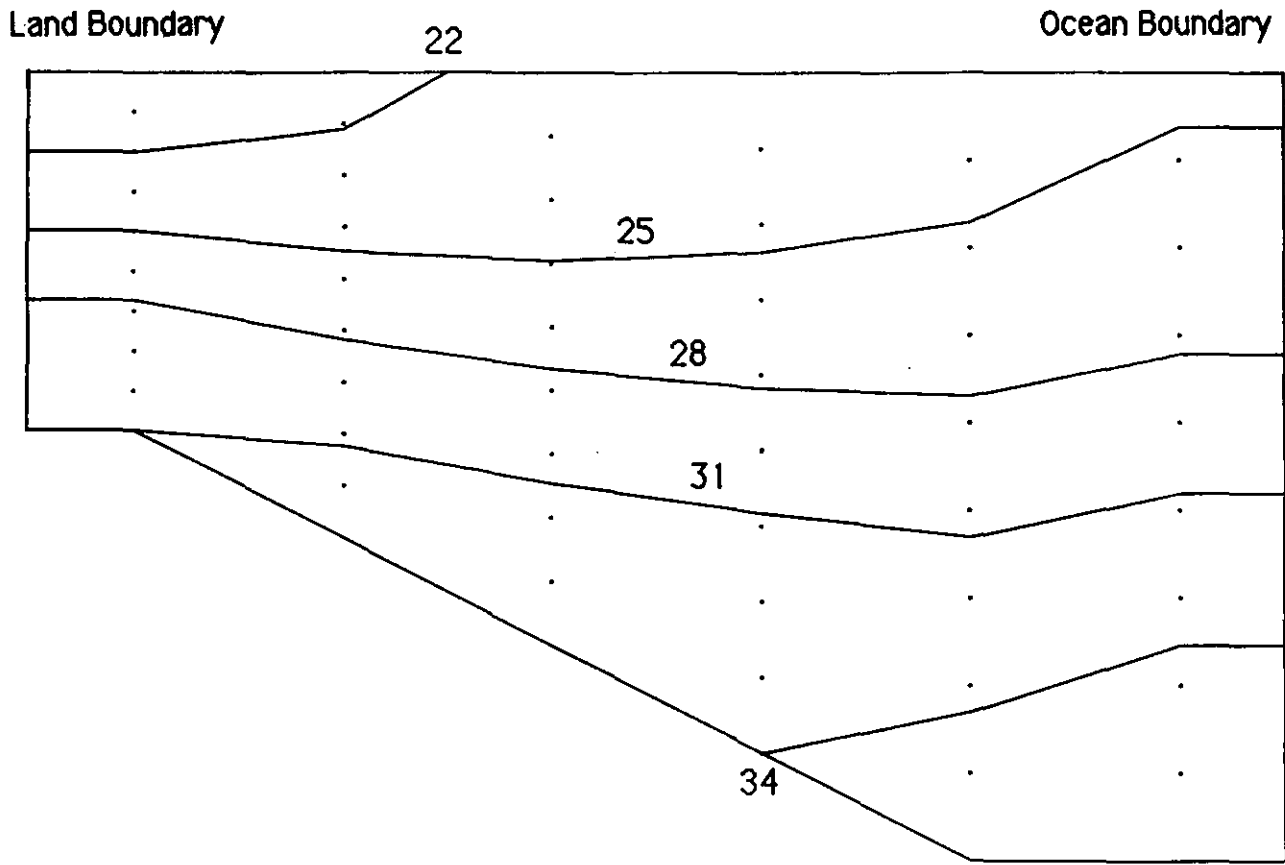


Figure 14. Oceanic boundary conditions for salinity. Units are parts per thousand.

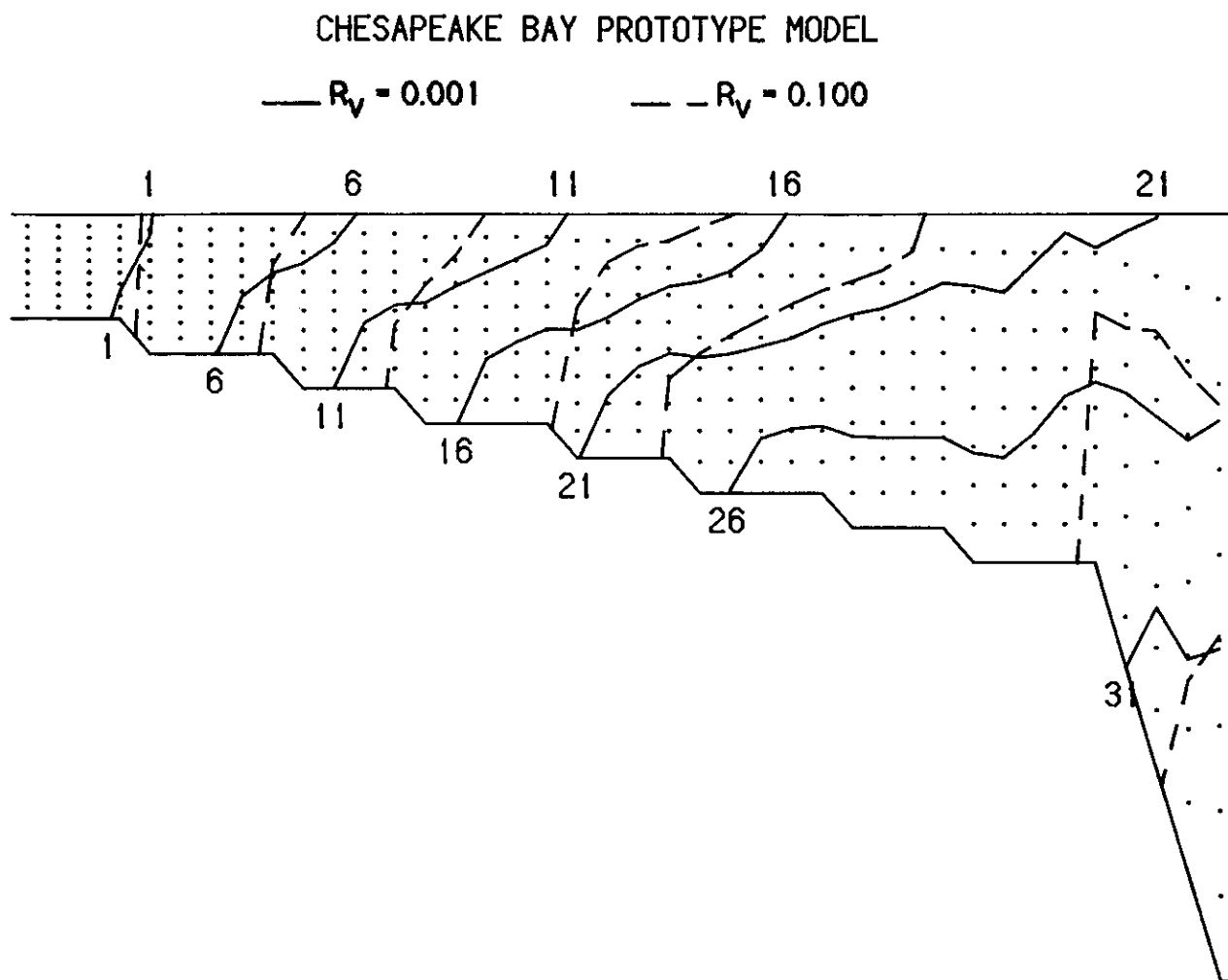


Figure 15. Cross-sectional distribution of salinity for the cases of $R_v=0.001, 0.100$.

CHESAPEAKE BAY PROTOTYPE MODEL

— $D_h = 100 \text{ m}^2/\text{s}$ - - $D_h = 1000 \text{ m}^2/\text{s}$

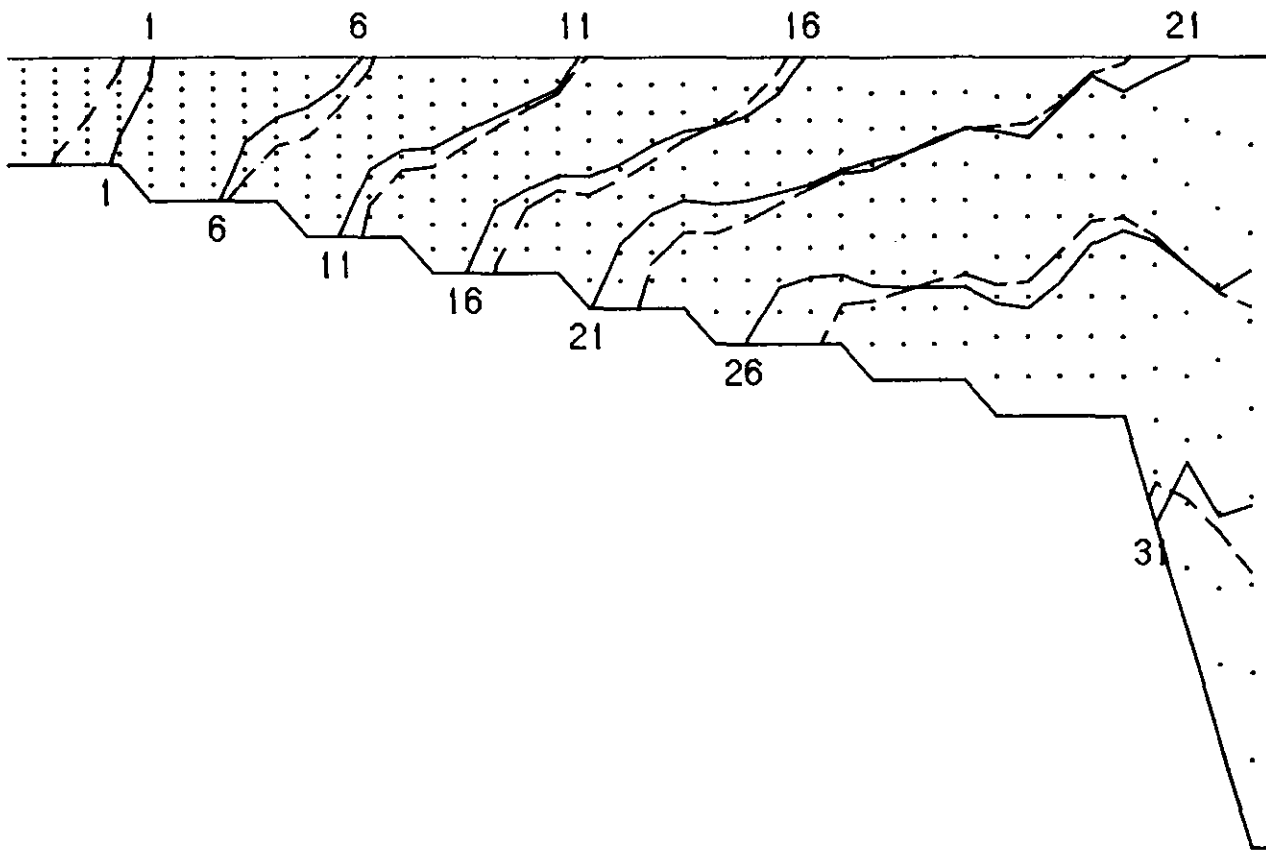


Figure 16. Same as Fig. 15, but for $D_h = 100, 1000 \text{ m}^2/\text{s}$.

CHESAPEAKE BAY PROTOTYPE MODEL

— Isohalines for 0000 6/21 - - - Isohalines for 0000 6/30

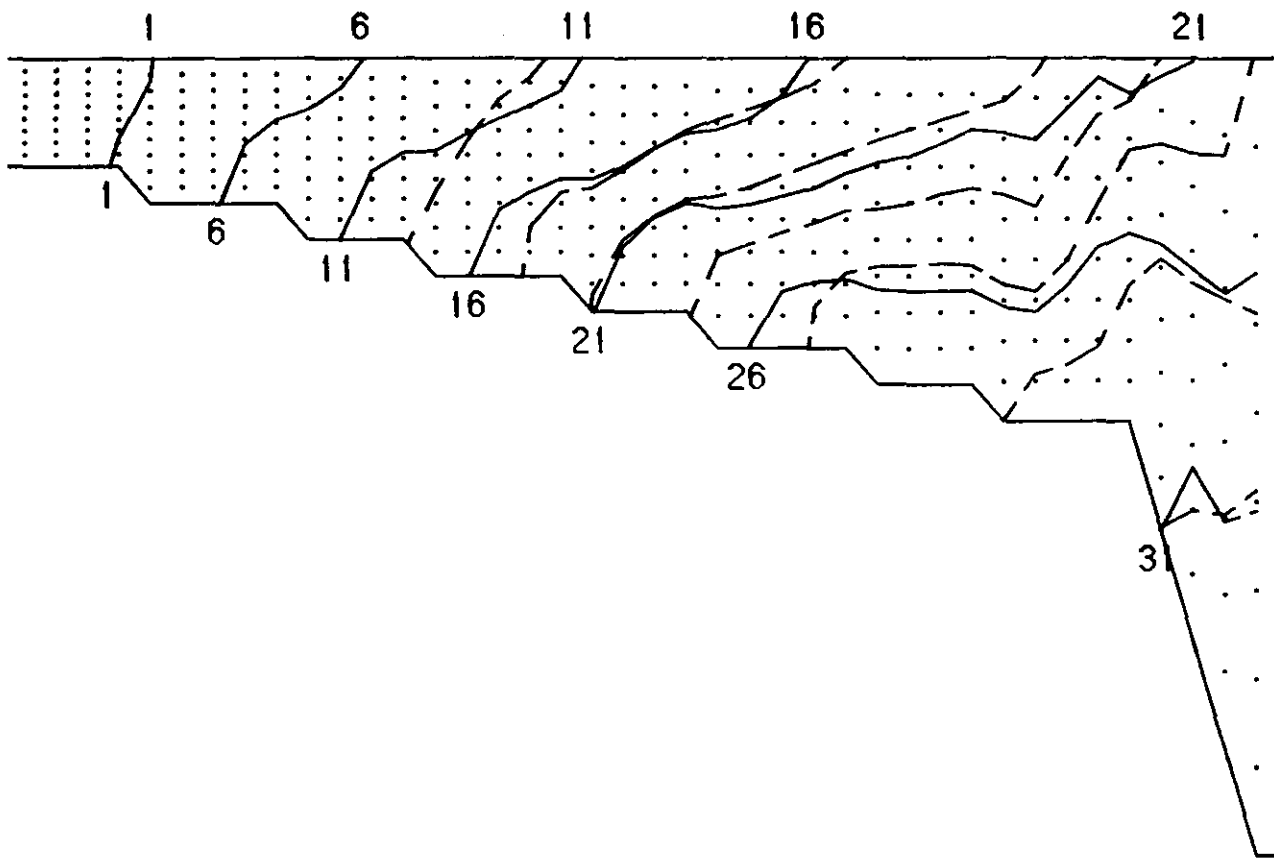


Figure 17. Salinity distribution at the start (solid lines) and after 9 days of simulation (0000 6/30) (dashed lines) with river flows simulating those from hurricane Agnes. The salinity displacement was at the maximum at the ninth day.

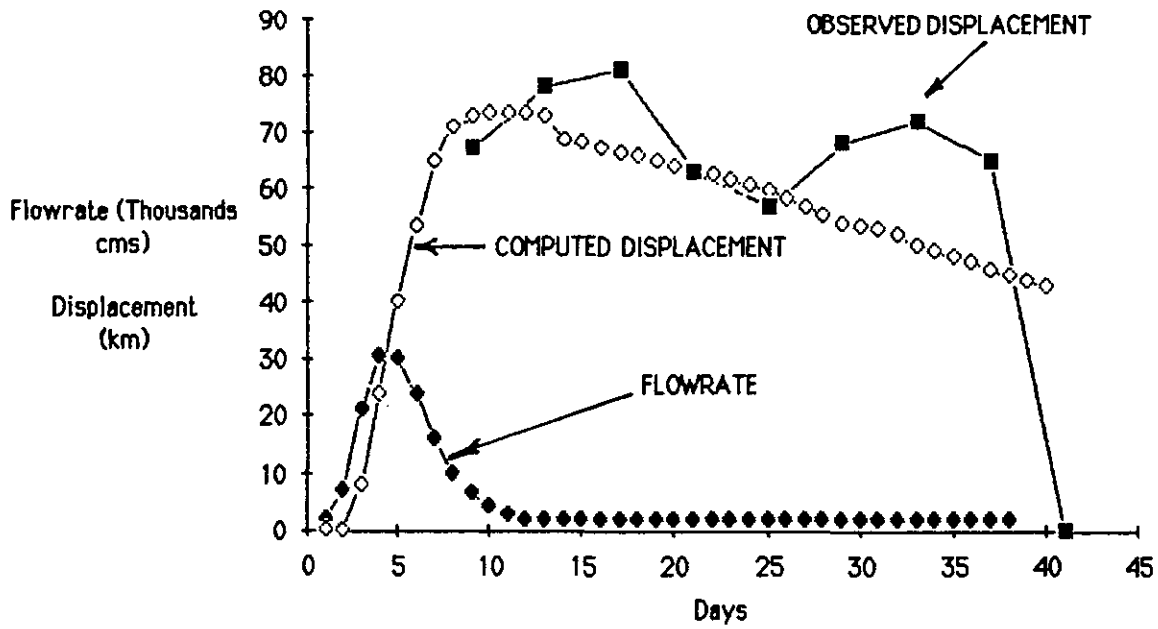


Figure 18. Susquehanna River flowrates (thousands of m^3/s) from hurricane Agnes, and the modeled and observed displacement (km) of the 5 ppt isohaline down the Bay.

